Electronic supplementary information

Chiral diketopyrrolo[3,4-*c*]pyrrole dyes with different substitution symmetry: impact of adamantyl groups on the photo-physical properties in solution and thin films

Martin Cigánek,[a] Claudio Vatteroni,[b] Francesca Romana Lauro,[b] Francesco Zinna,[b] Gennaro Pescitelli,[b] Jozef Krajčovič,*[a] Gianluigi Albano*[b,c]

[a] *Faculty of Chemistry, Brno University of Technology, Purkyňova 118, 612 00, Brno, Czech Republic*
[b] *Dipartimento di Chimica e Chimica Industriale, Università di Pisa, Via Giuseppe Moruzzi 13, 56124 Pisa, Italy*
[c] *Dipartimento di Scienze Chimiche, della Vita e della Sostenibilità Ambientale, Università degli Studi di Parma, Parco Area delle Scienze, 17/A, 43124 Parma, Italy*

*E-mail: krajcovic@fch.vut.cz, gianluigi.albano@unipr.it

Table of contents

Supplementary Figures

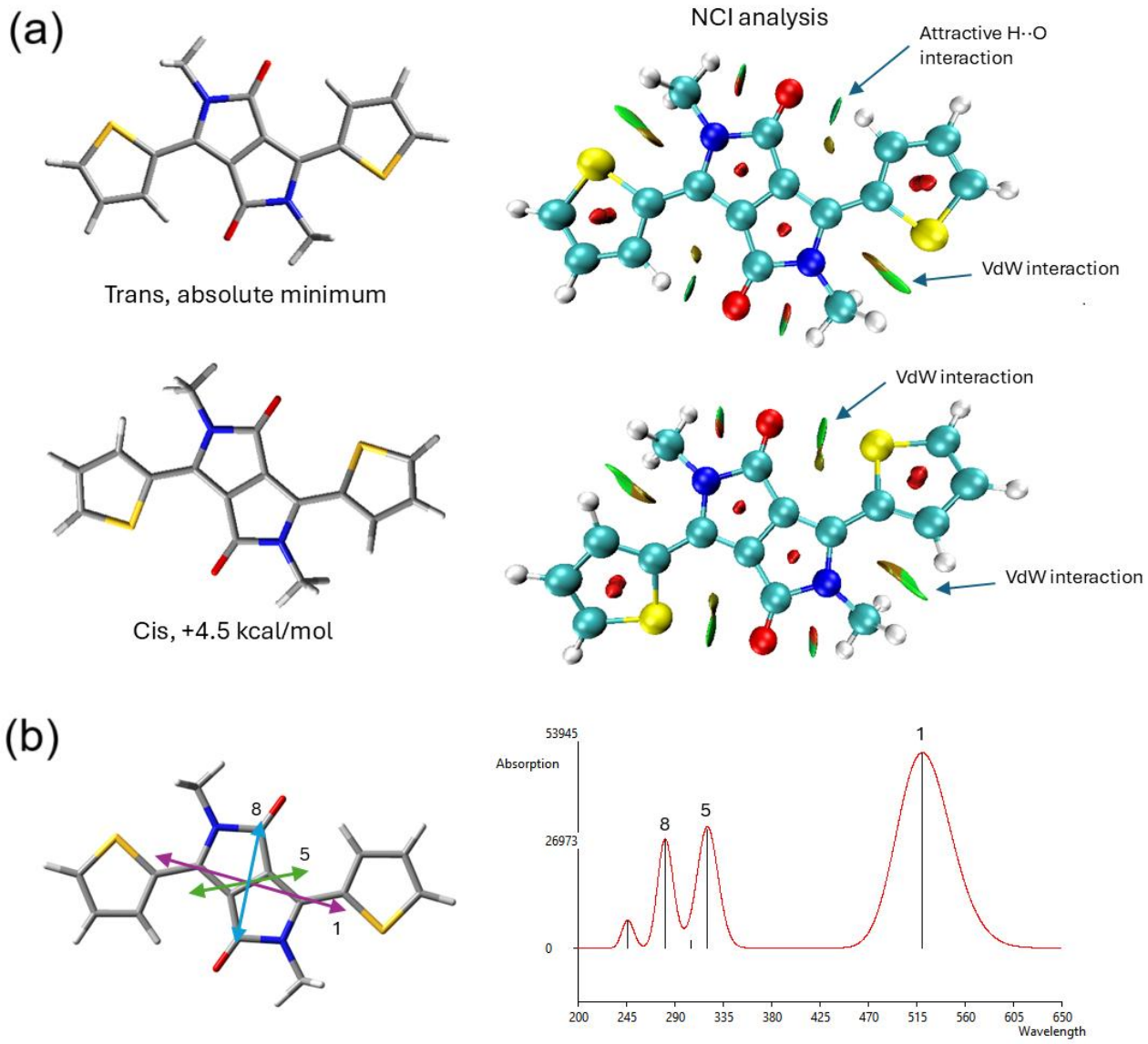

Figure S1.

(a) Left: DFT-optimized geometries for the two isomers of model **DPP-Me** at B3LYP-D3BJ/6-311+G(d,p) level. Right: Non-covalent interaction analysis run with MultiWfn showing green areas for attractive Van der Waals interactions. (b) TD-DFT calculated UV spectrum (gaussian σ 0.2 eV) on **DPP-Me** and major transition dipole moment directions calculated at B3LYP/def2-TZVP level.

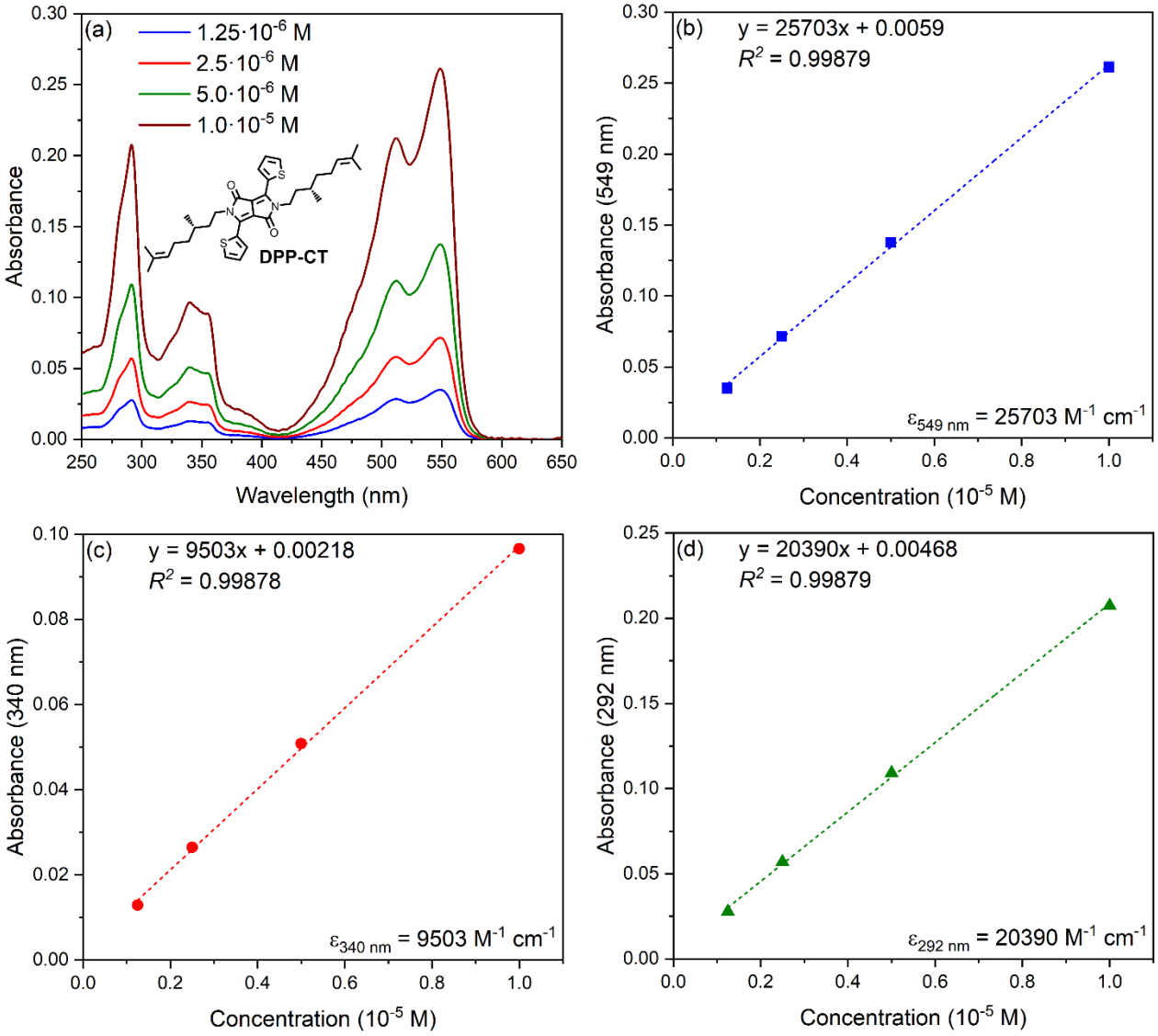

Figure S2.

Determination of molar extinction coefficients ε of **DPP-CT** dye **1** in $CHCl_3$ solution: (a) UV-Vis absorbance spectra at different concentrations (from $1.25 \cdot 10^{-6}$ M to $1.0 \cdot 10^{-5}$ M); (b) absorbance at 549 nm *vs.* concentration plot; (c) absorbance at 340 nm *vs.* concentration plot; (d) absorbance at 292 nm *vs.* concentration plot.

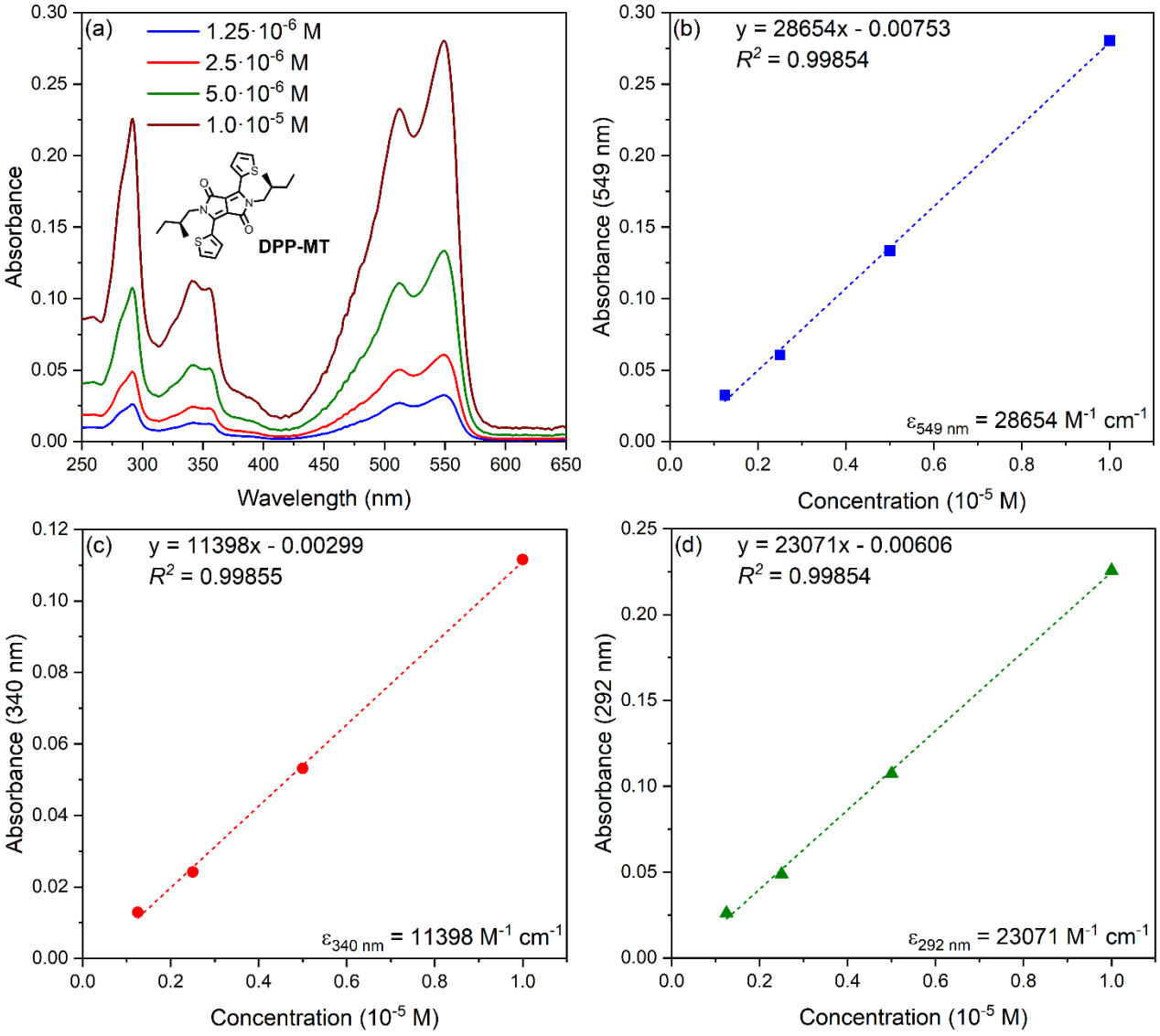

Figure S3.

Determination of molar extinction coefficients ε of **DPP-MT** dye **2** in $CHCl_3$ solution: (a) UV-Vis absorbance spectra at different concentrations (from $1.25 \cdot 10^{-6}$ M to $1.0 \cdot 10^{-5}$ M); (b) absorbance at 549 nm *vs.* concentration plot; (c) absorbance at 340 nm *vs.* concentration plot; (d) absorbance at 292 nm *vs.* concentration plot.

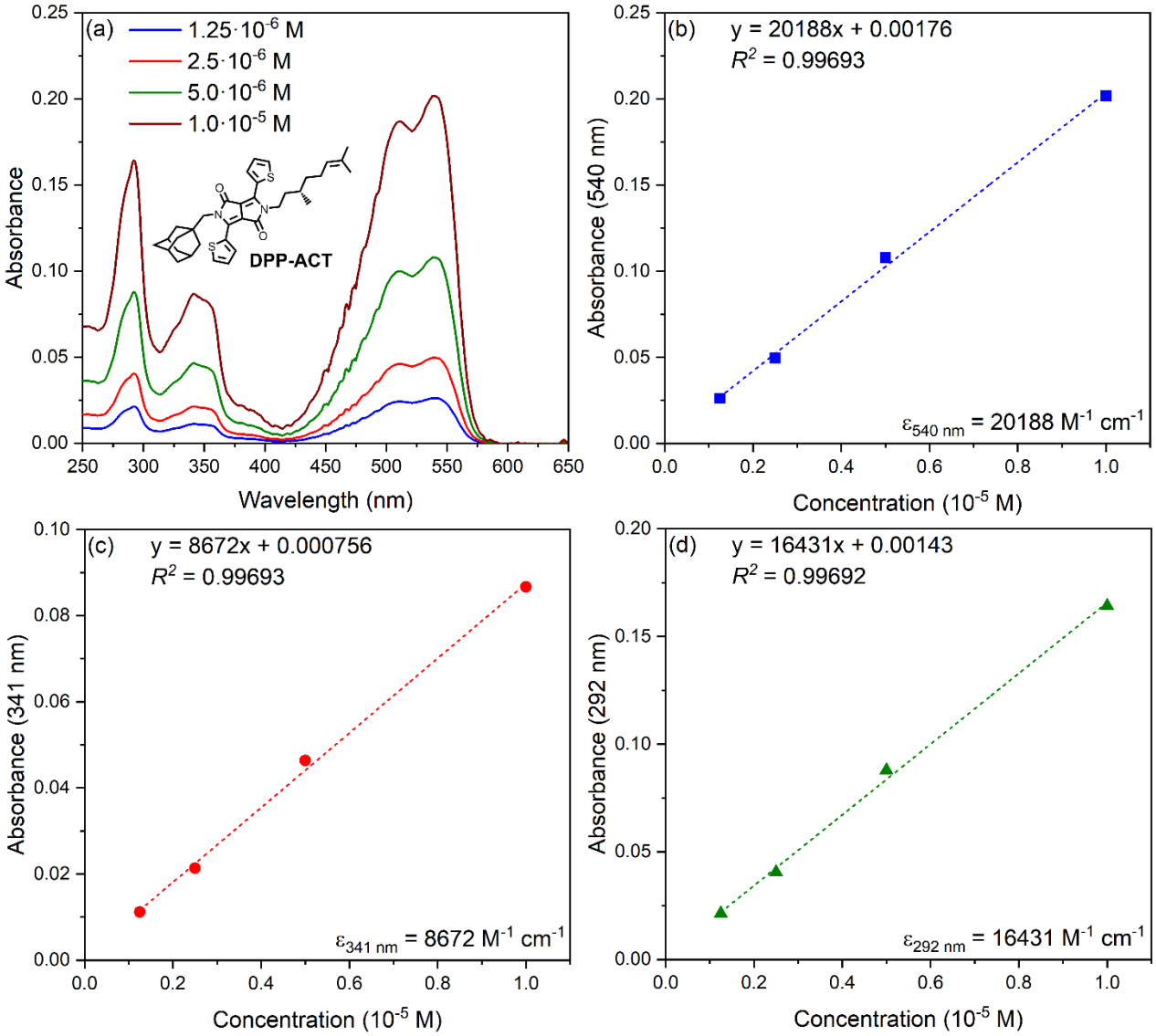

Figure S4.

Determination of molar extinction coefficients ε of **DPP-ACT** dye **3** in $CHCl_3$ solution: (a) UV-Vis absorbance spectra at different concentrations (from $1.25 \cdot 10^{-6}$ M to $1.0 \cdot 10^{-5}$ M); (b) absorbance at 540 nm *vs.* concentration plot; (c) absorbance at 341 nm *vs.* concentration plot; (d) absorbance at 292 nm *vs.* concentration plot.

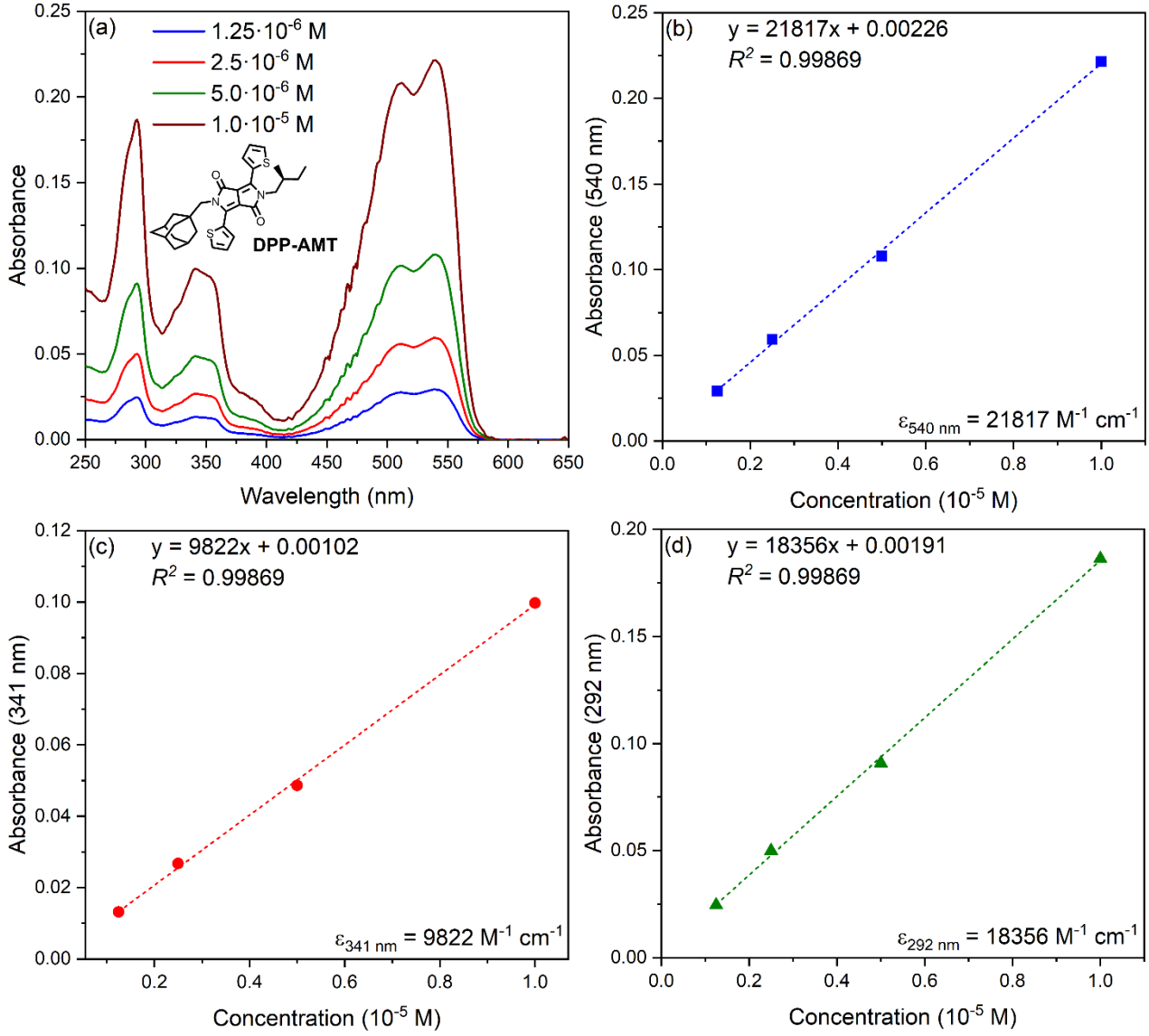

Figure S5.

Determination of molar extinction coefficients ε of **DPP-AMT** dye **4** in $CHCl_3$ solution: (a) UV-Vis absorbance spectra at different concentrations (from $1.25 \cdot 10^{-6}$ M to $1.0 \cdot 10^{-5}$ M); (b) absorbance at 540 nm *vs.* concentration plot; (c) absorbance at 341 nm *vs.* concentration plot; (d) absorbance at 292 nm *vs.* concentration plot.

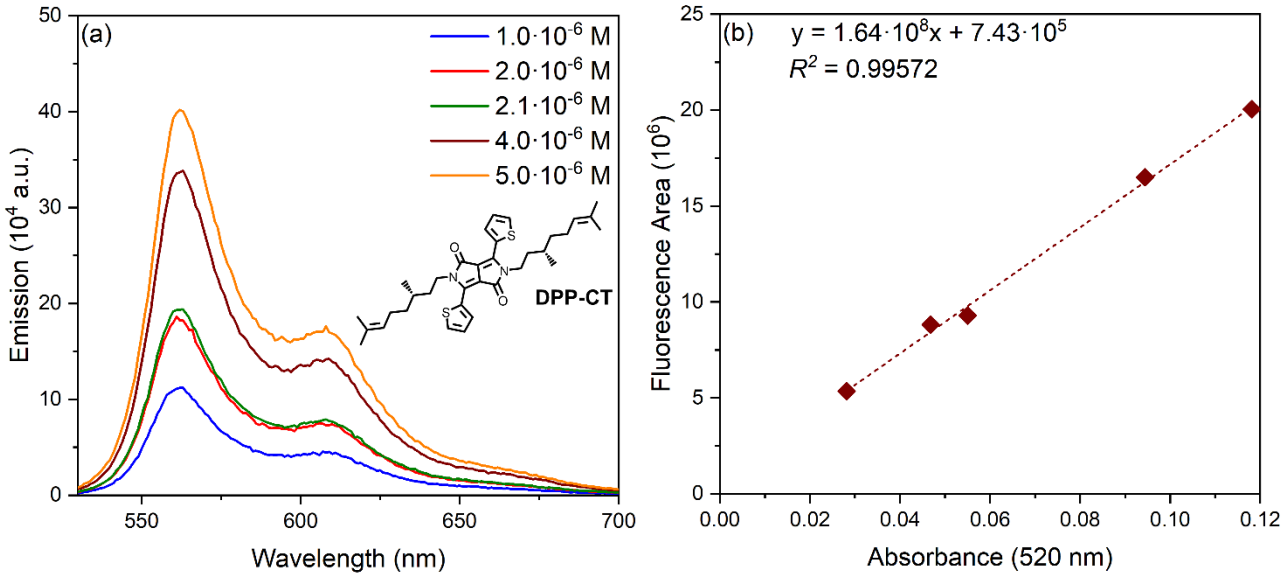

Figure S6.

Determination of fluorescence quantum yield ϕ of **DPP-CT** dye **1** in $CHCl_3$ solution: (a) photoluminescence emission spectra at different concentrations (from $1.0 \cdot 10^{-6}$ M to $5.0 \cdot 10^{-6}$ M), excitation wavelength 520 nm; (b) integrated fluorescence area *vs.* absorbance at 520 nm plot.

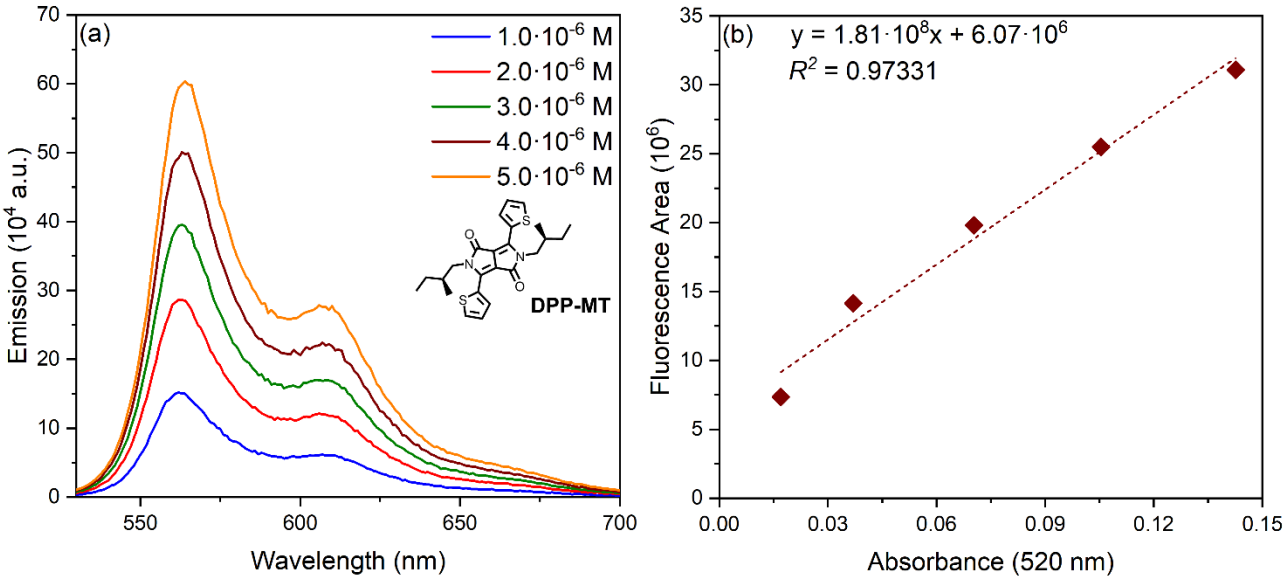

Figure S7.

Determination of fluorescence quantum yield ϕ of **DPP-MT** dye **2** in $CHCl_3$ solution: (a) photoluminescence emission spectra at different concentrations (from $1.0 \cdot 10^{-6}$ M to $5.0 \cdot 10^{-6}$ M), excitation wavelength 520 nm; (b) integrated fluorescence area *vs.* absorbance at 520 nm plot.

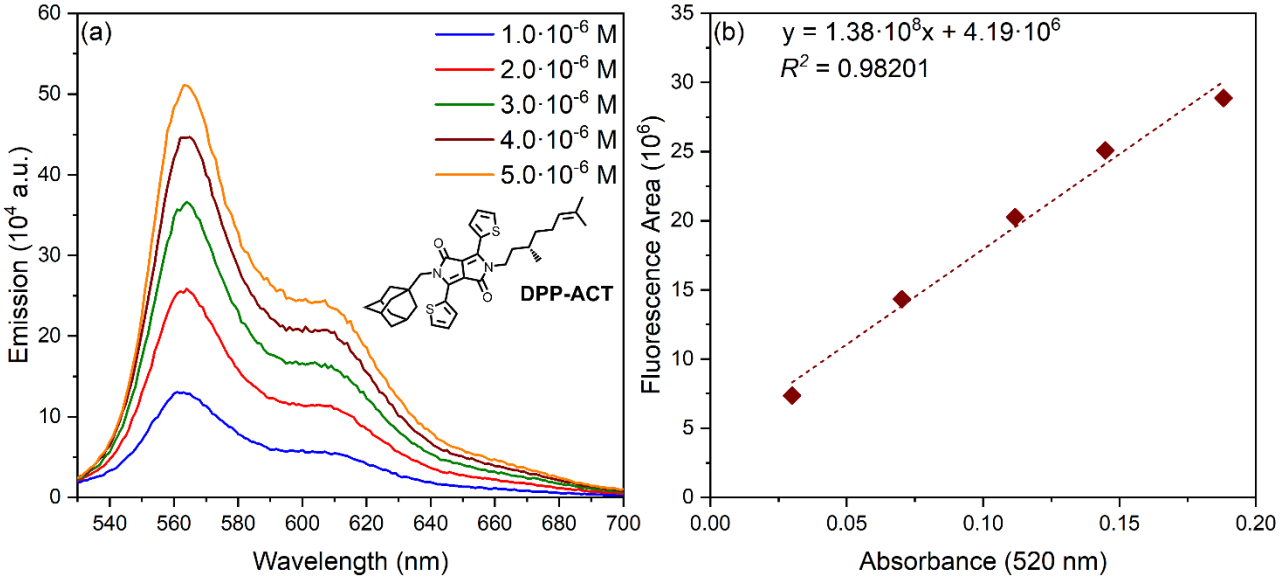

Figure S8.

Determination of fluorescence quantum yield ϕ of **DPP-ACT** dye **3** in $CHCl_3$ solution: (a) photoluminescence emission spectra at different concentrations (from $1.0 \cdot 10^{-6}$ M to $5.0 \cdot 10^{-6}$ M), excitation wavelength 520 nm; (b) integrated fluorescence area *vs.* absorbance at 520 nm plot.

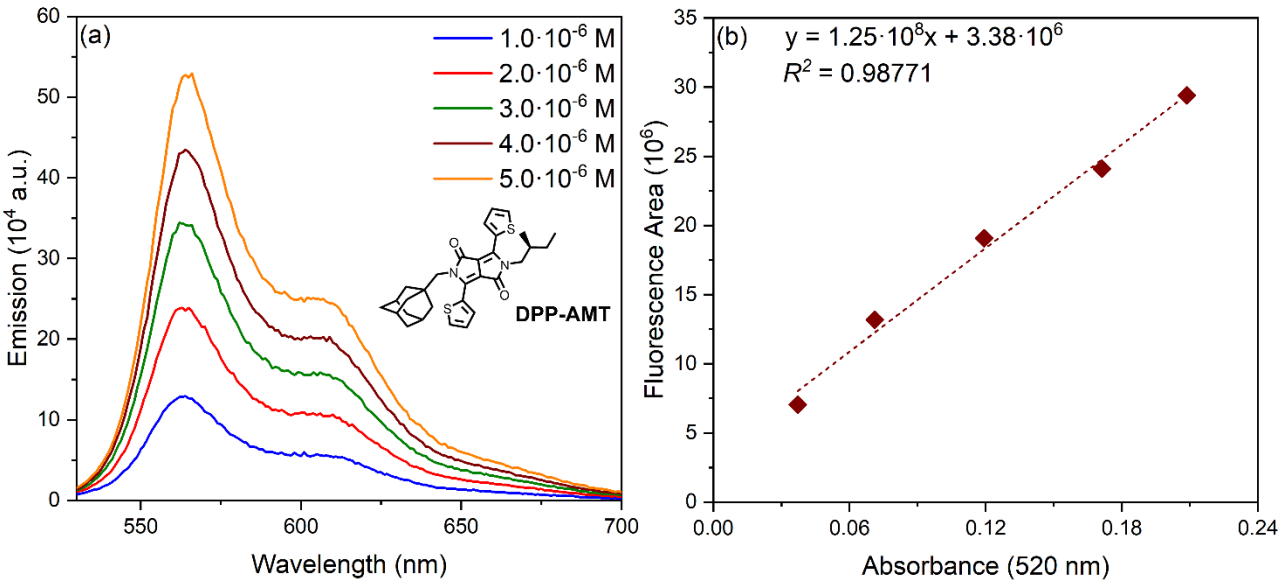

Figure S9.

Determination of fluorescence quantum yield ϕ of **DPP-AMT** dye **4** in $CHCl_3$ solution: (a) photoluminescence emission spectra at different concentrations (from $1.0 \cdot 10^{-6}$ M to $5.0 \cdot 10^{-6}$ M), excitation wavelength 520 nm; (b) integrated fluorescence area *vs.* absorbance at 520 nm plot.

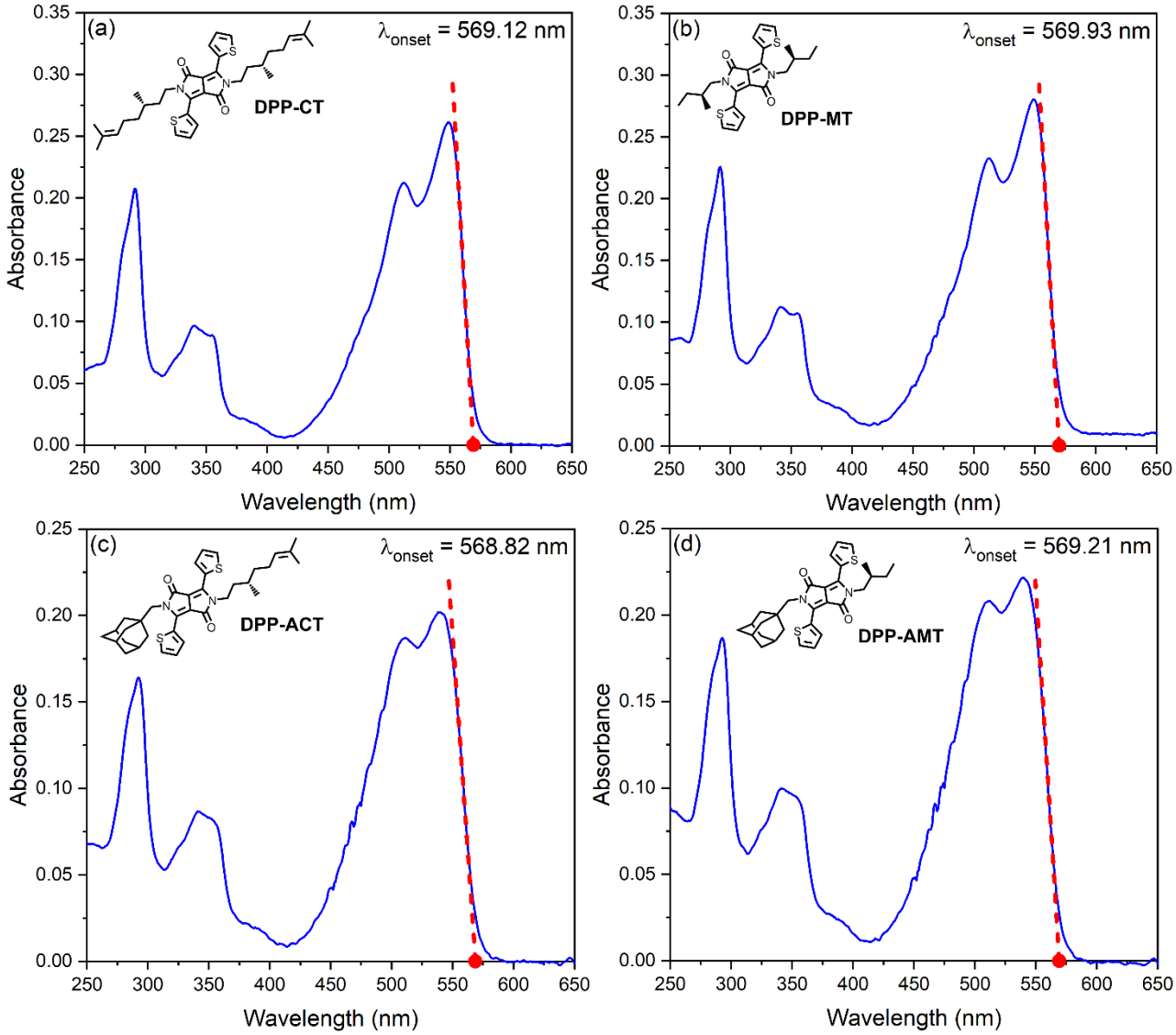

Figure S10.

Determination of absorbance onset wavelengths λ_{onset} of chiral DPP dyes **1–4** in $CHCl_3$ solution, obtained from the intercept of the red-side slope of the absorbance main band with the wavelength axis: (a) **DPP-CT**; (b) **DPP-MT**; (c) **DPP-ACT**; (d) **DPP-AMT**.

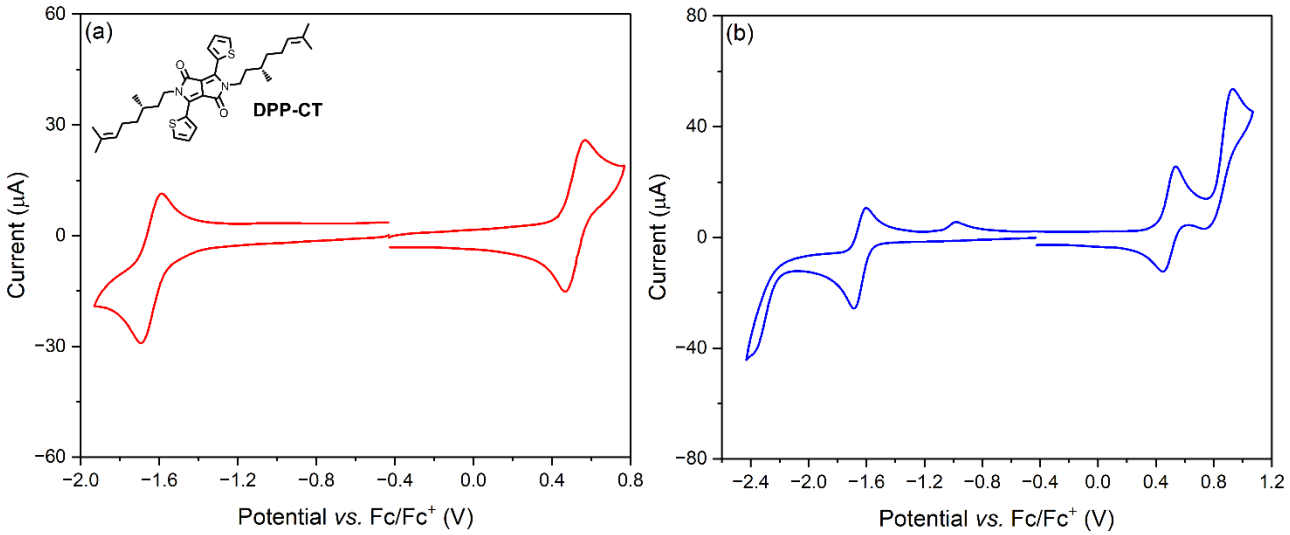

Figure S11.

Cyclic voltammograms of **DPP-CT** dye **1** in a CH_2Cl_2/*n*-Bu_4NPF_6 0.2 M solution, recorded on a Pt disk (surface: 0.07 cm^2) working electrode in the potential range between: (a) the first oxidation and the first reduction; (b) the second oxidation and the second reduction. Sample concentration 10^{-3} M; scanning rate 100 mV s^{-1}.

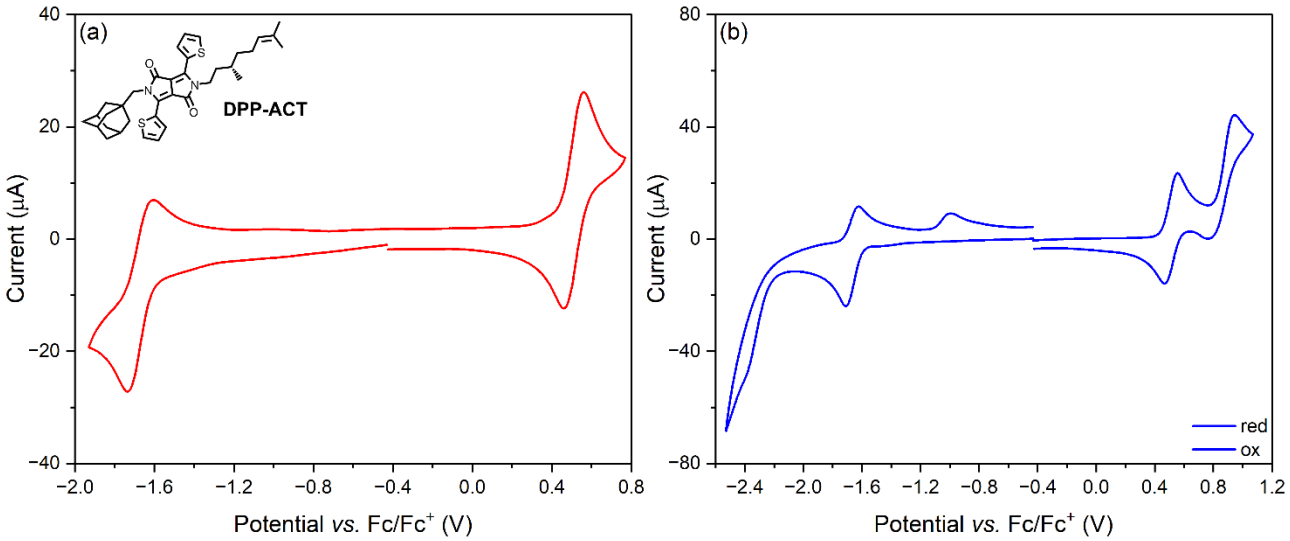

Figure S12.

Cyclic voltammograms of **DPP-ACT** dye **3** in a CH_2Cl_2/*n*-Bu_4NPF_6 0.2 M solution, recorded on a Pt disk (surface: 0.07 cm^2) working electrode in the potential range between: (a) the first oxidation and the first reduction; (b) the second oxidation and the second reduction. Sample concentration 10^{-3} M; scanning rate 100 mV s^{-1}.

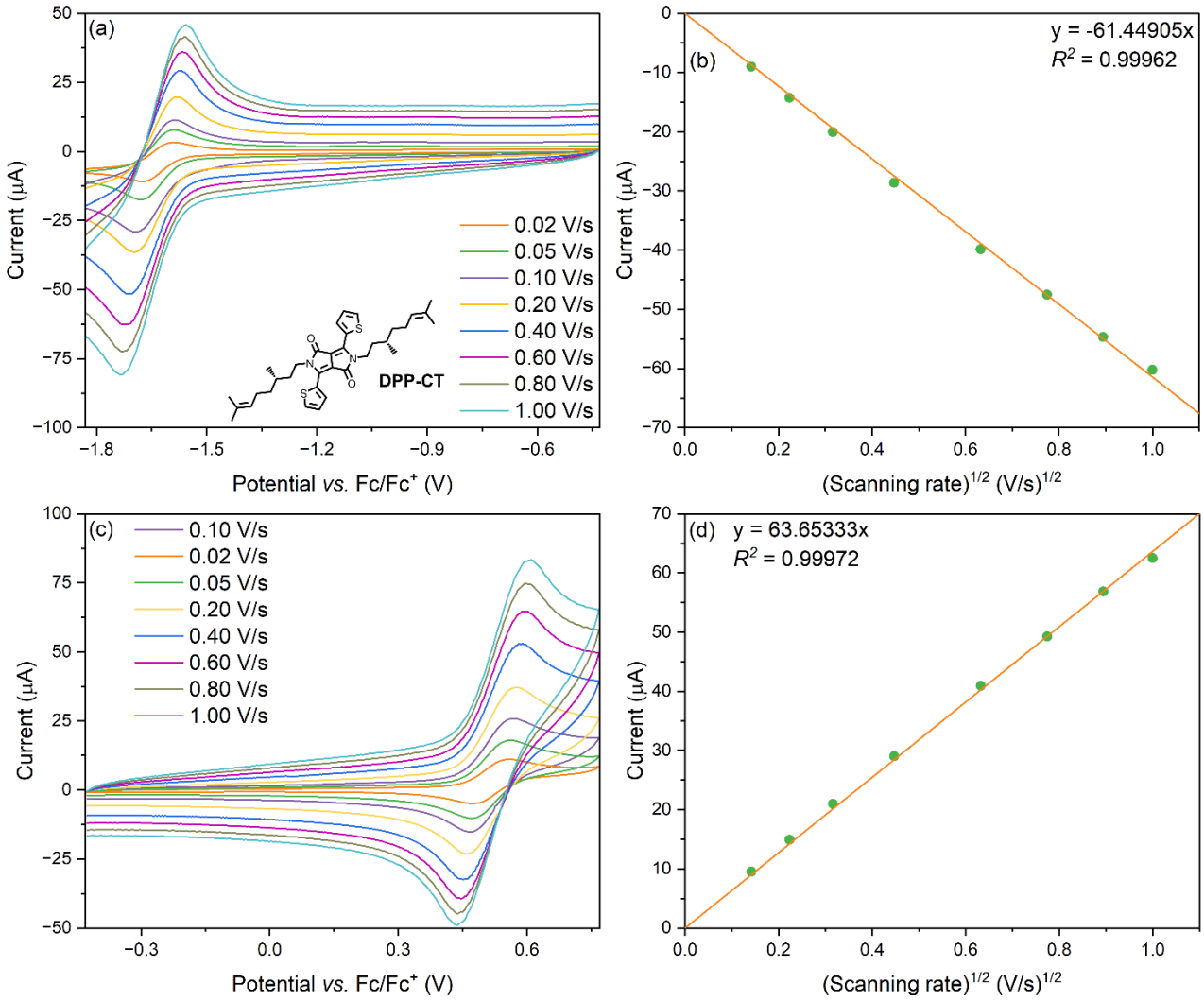

Figure S13.

Cyclic voltammetry measurements of **DPP-CT** dye **1** in a CH_2Cl_2/*n*-Bu_4NPF_6 0.2 M solution, recorded on a Pt disk (surface: 0.07 cm^2) working electrode at different scanning rate (between 10 mV s^{-1} and 1000 mV s^{-1}). (a) Cyclic voltammograms for the first reduction process and (b) corresponding cathodic peak current *vs.* scanning rate plot. (c) Cyclic voltammograms for the first oxidation process and (d) corresponding anodic peak current *vs.* scanning rate plot.

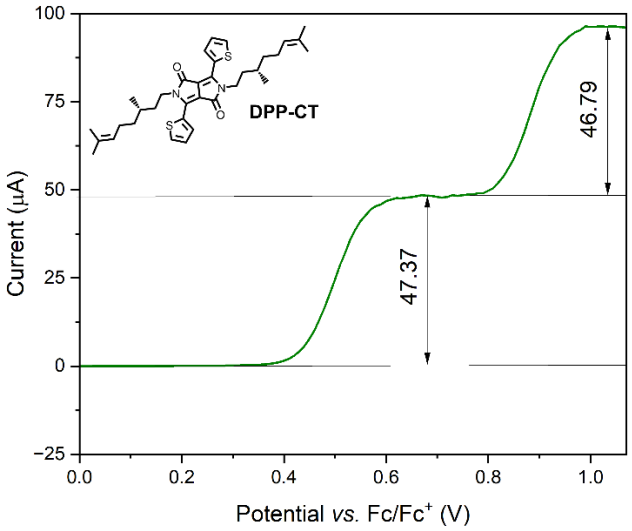

Figure S14.

Linear sweep voltammetry measurements of **DPP-CT** dye **1** in a CH_2Cl_2/*n*-Bu_4NPF_6 0.2 M solution, recorded on a Pt rotating disk (surface: 0.07 cm²) working electrode. Sample concentration 10^{-3} M; scanning rate 20 mV s^{-1}.

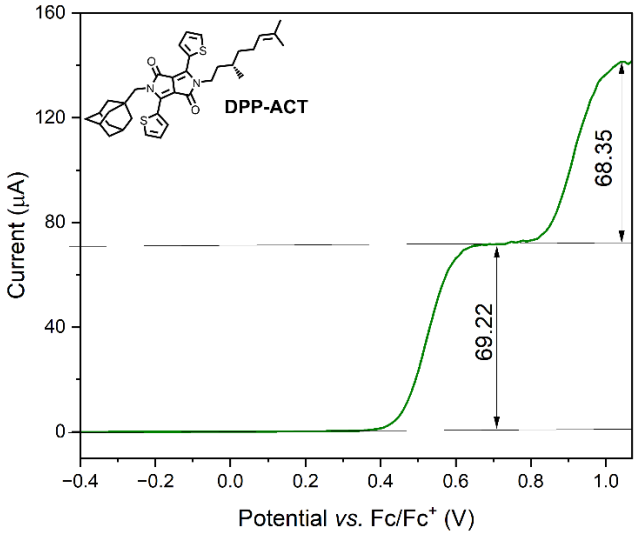

Figure S15.

Linear sweep voltammetry measurements of **DPP-ACT** dye **3** in a CH_2Cl_2/*n*-Bu_4NPF_6 0.2 M solution, recorded on a Pt rotating disk (surface: 0.07 cm²) working electrode. Sample concentration 10^{-3} M; scanning rate 20 mV s^{-1}.

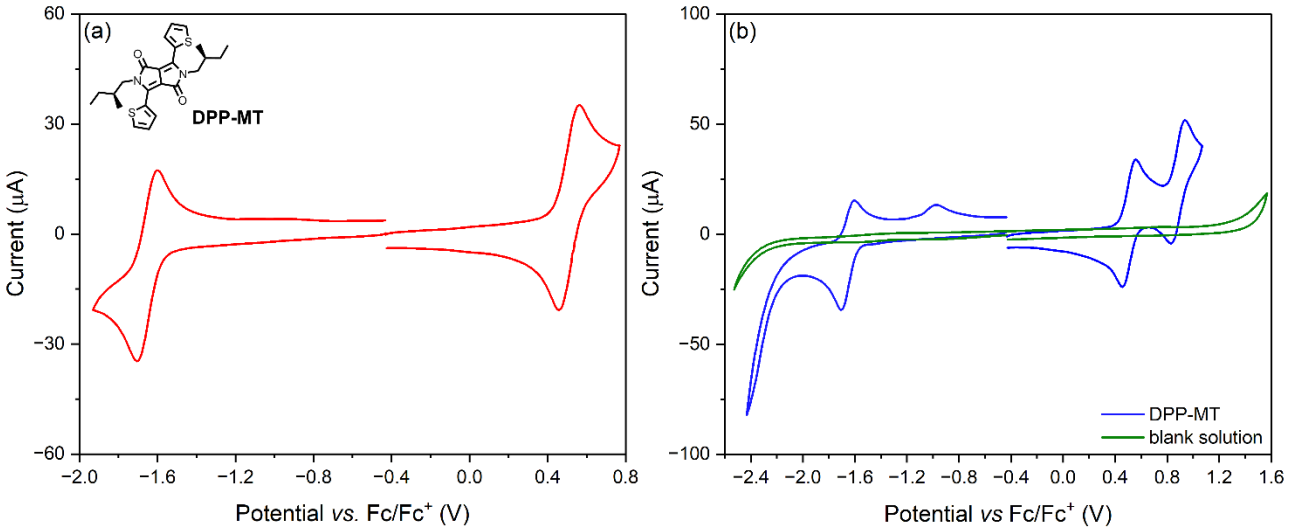

Figure S16.

Cyclic voltammograms in a CH_2Cl_2/*n*-Bu_4NPF_6 0.2 M solution, recorded on a Pt disk (surface: 0.07 cm^2) working at a scan rate of 100 mV s^{-1}. (a) Voltammogram of **DPP-MT** dye **2** (1.0×10^{-3} M), showing the first oxidation and first reduction processes. (b) Voltammogram of **DPP-MT** dye **2** (1.0×10^{-3} M, blue line) compared with the blank solution (CH_2Cl_2 with 0.2 M *n*-Bu_4NPF_6, green line), recorded in the potential range up to the second oxidation and second reduction.

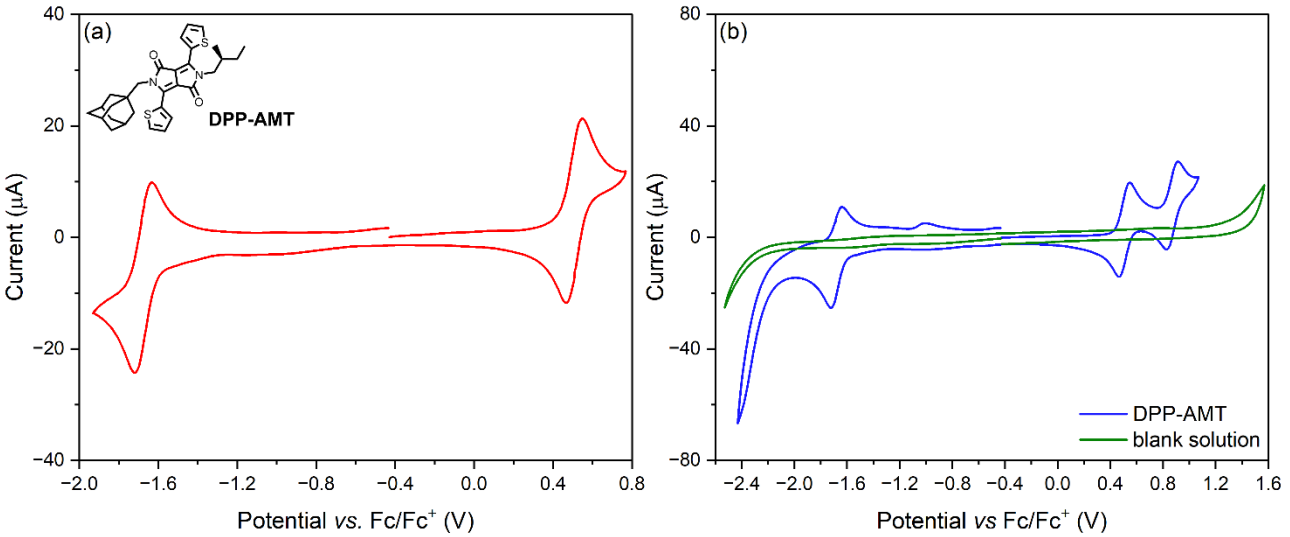

Figure S17.

Cyclic voltammograms in a CH_2Cl_2/*n*-Bu_4NPF_6 0.2 M solution, recorded on a Pt disk (surface: 0.07 cm^2) working electrode at a scan rate of 100 mV s^{-1}. (a) Voltammogram of **DPP-AMT** dye **4** (1.0×10^{-3} M), showing the first oxidation and first reduction processes. (b) Voltammogram of **DPP-AMT** dye **4** (1.0×10^{-3} M, blue line) compared with the blank solution (CH_2Cl_2 with 0.2 M n-Bu_4NPF_6, green line), recorded in the potential range up to the second oxidation and second reduction.

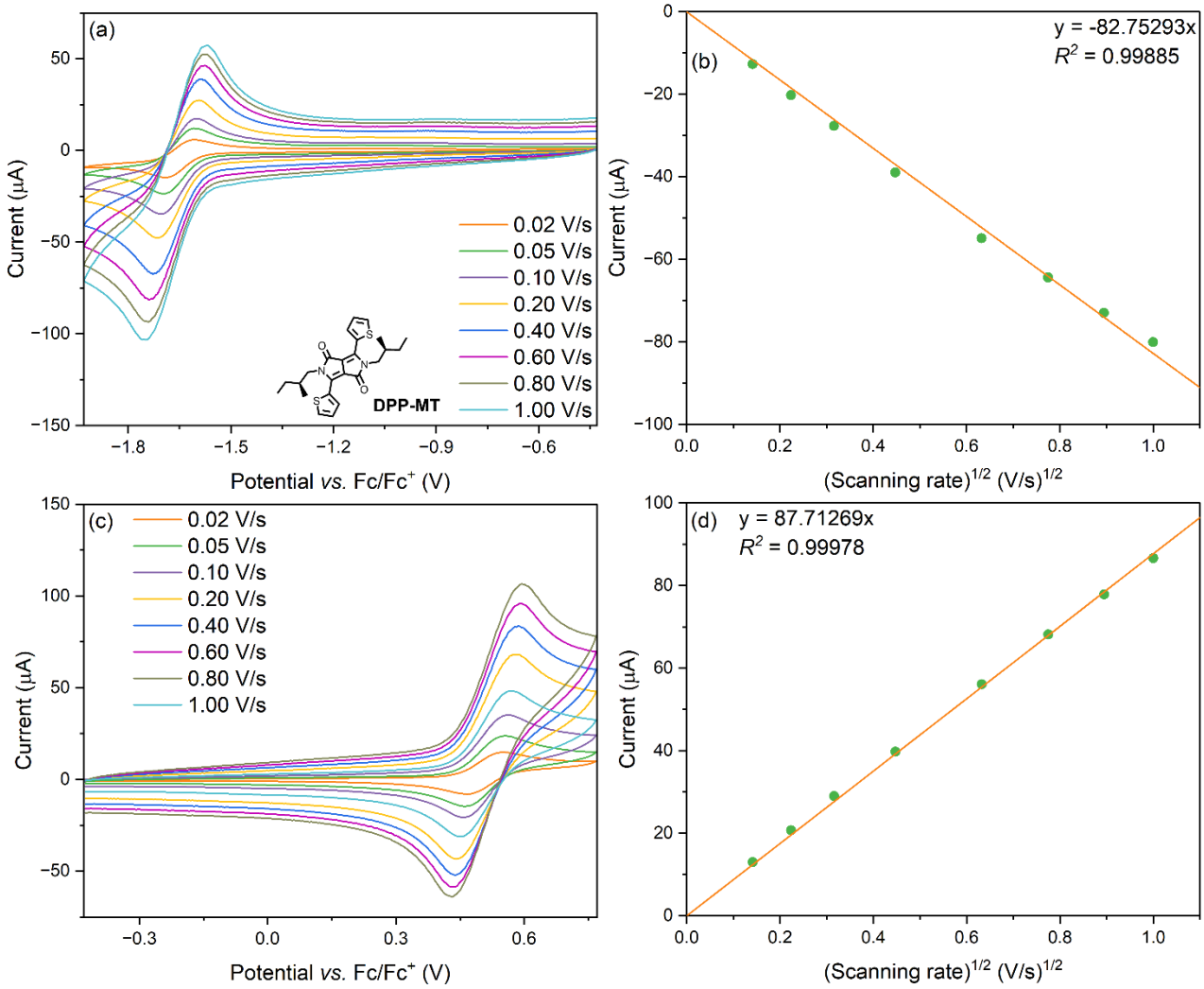

Figure S18.

Cyclic voltammetry measurements of **DPP-MT** dye **2** in a CH_2Cl_2/*n*-Bu_4NPF_6 0.2 M solution, recorded on a Pt disk (surface: 0.07 cm²) working electrode at different scanning rate (between 10 mV s^{-1} and 1000 mV s^{-1}). (a) Cyclic voltammograms for the first reduction process and (b) corresponding cathodic peak current *vs.* scanning rate plot. (c) Cyclic voltammograms for the first oxidation process and (d) corresponding anodic peak current *vs.* scanning rate plot.

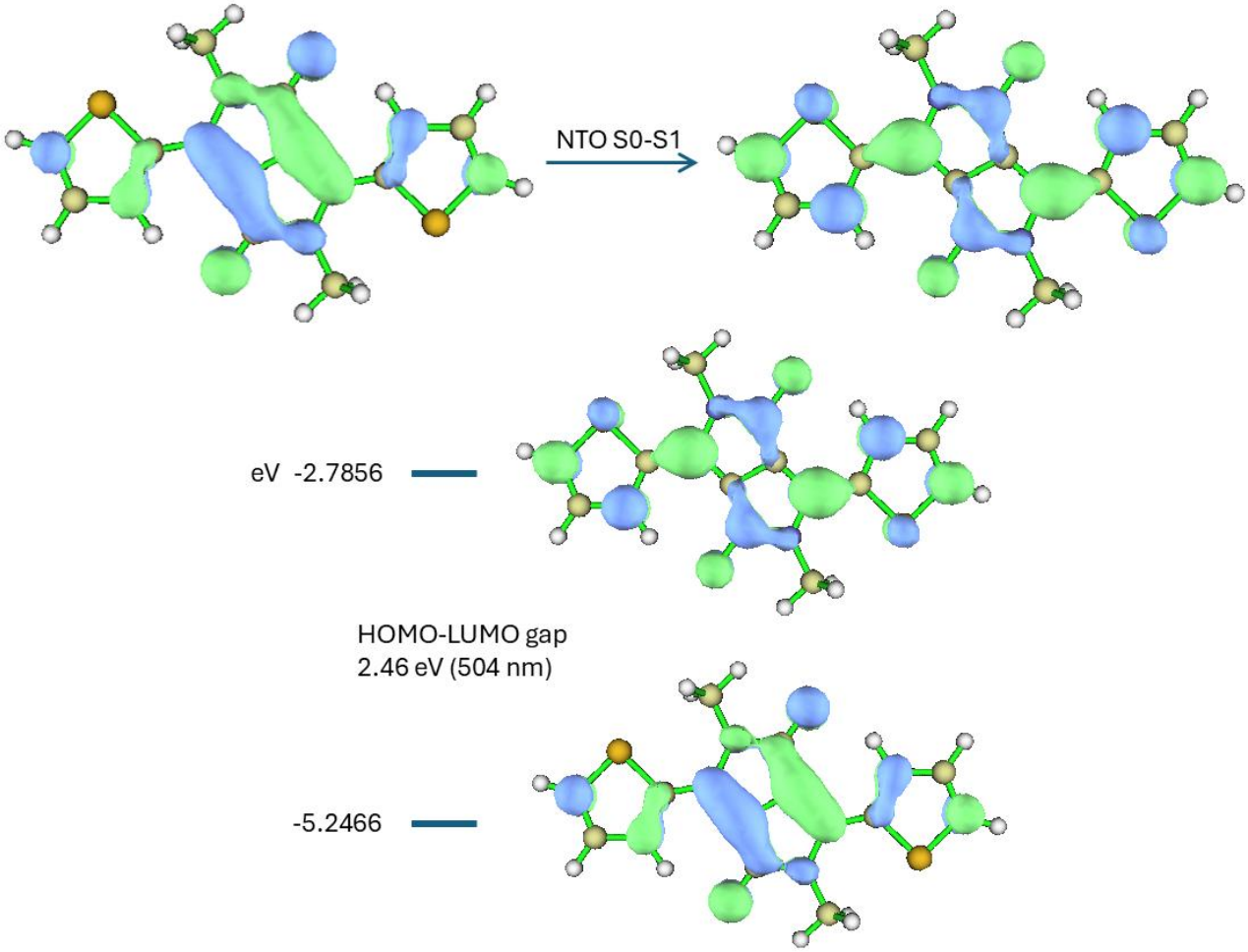

Figure S19.

Top: Natural Transition Orbital analysis involved in the 1st calculated transition for model **DPP-Me** at B3LYP/def2-TZVP level (isovalue 0.04). Bottom: HOMO/LUMO plots (isovalue 0.04), energy levels and HOMO-LUMO gap.

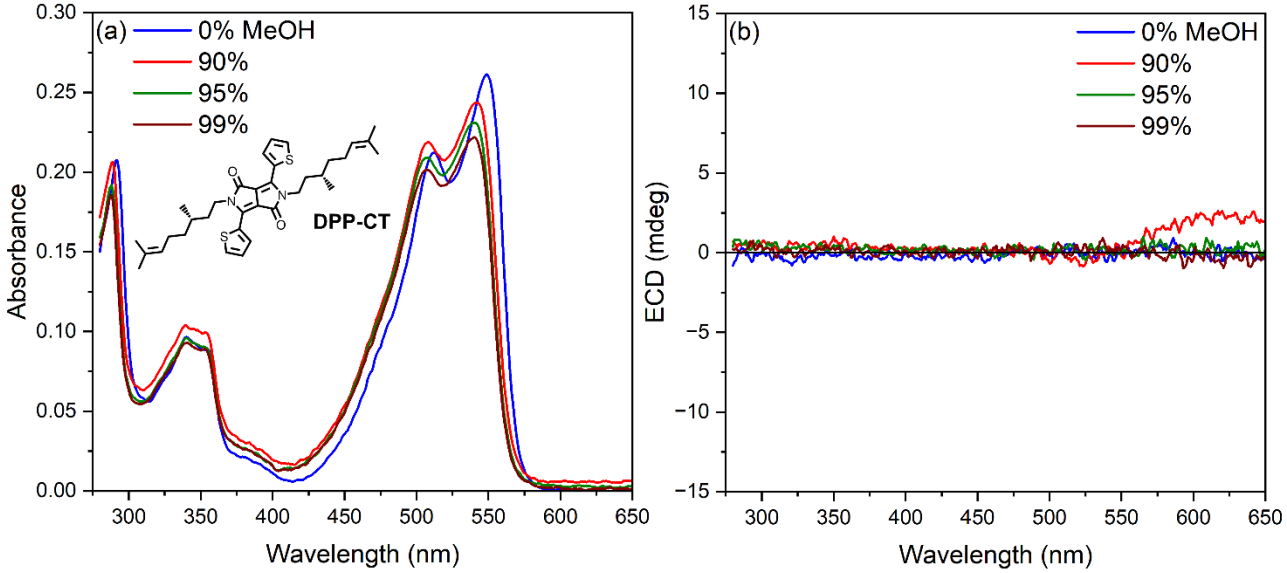

Figure S20.

Optical and chiroptical investigation of **DPP-CT** dye **1** under condition of solution aggregation: (a) UV-Vis absorbance spectra and (b) ECD spectra in $CHCl_3$/MeOH mixtures with increasing amounts of MeOH (from 0% to 99%). Cell length 1 cm; sample concentration 10^{-5} M.

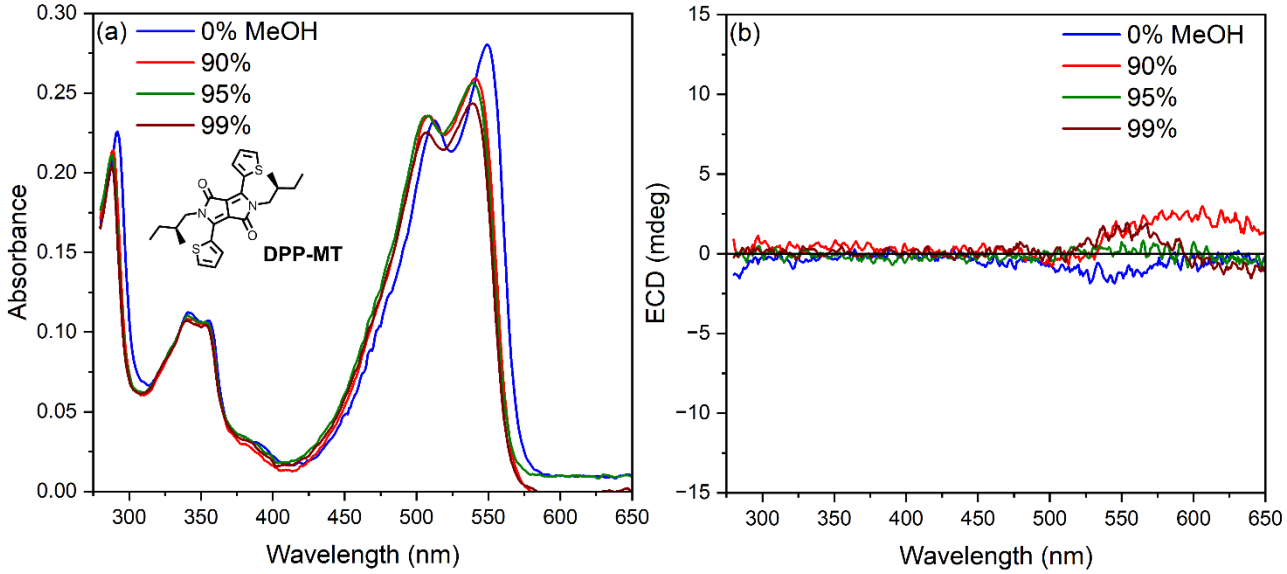

Figure S21.

Optical and chiroptical investigation of **DPP-MT** dye **2** under condition of solution aggregation: (a) UV-Vis absorbance spectra and (b) ECD spectra in $CHCl_3$/MeOH mixtures with increasing amounts of MeOH (from 0% to 99%). Cell length 1 cm; sample concentration 10^{-5} M.

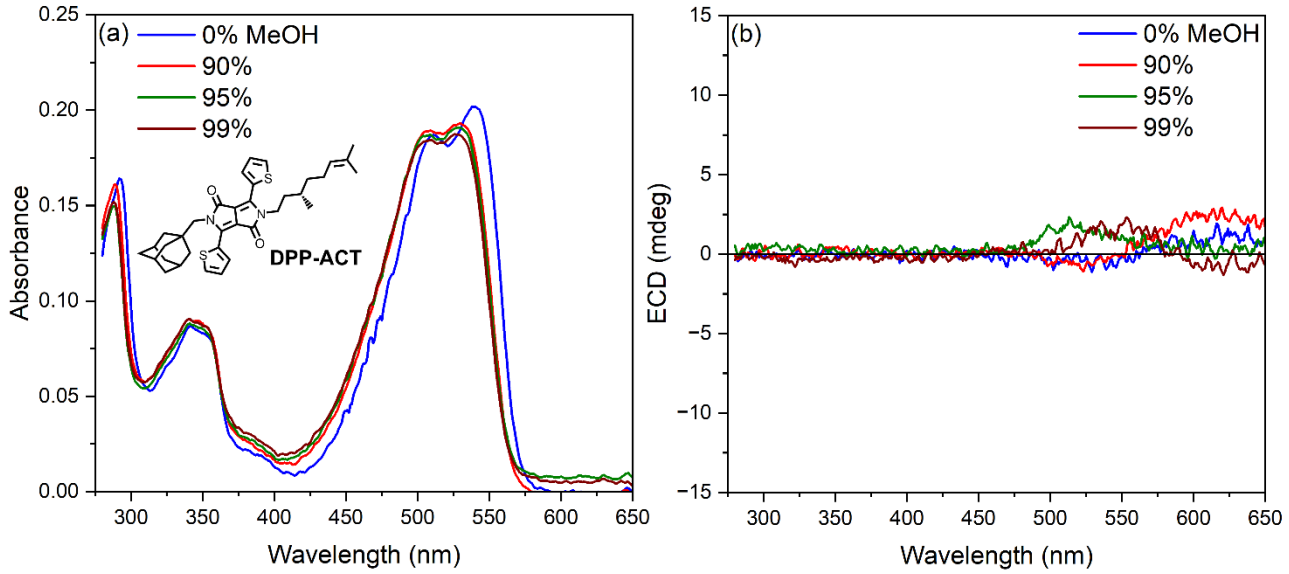

Figure S22.

Optical and chiroptical investigation of **DPP-ACT** dye **3** under condition of solution aggregation: (a) UV-Vis absorbance spectra and (b) ECD spectra in $CHCl_3$/MeOH mixtures with increasing amounts of MeOH (from 0% to 99%). Cell length 1 cm; sample concentration 10^{-5} M.

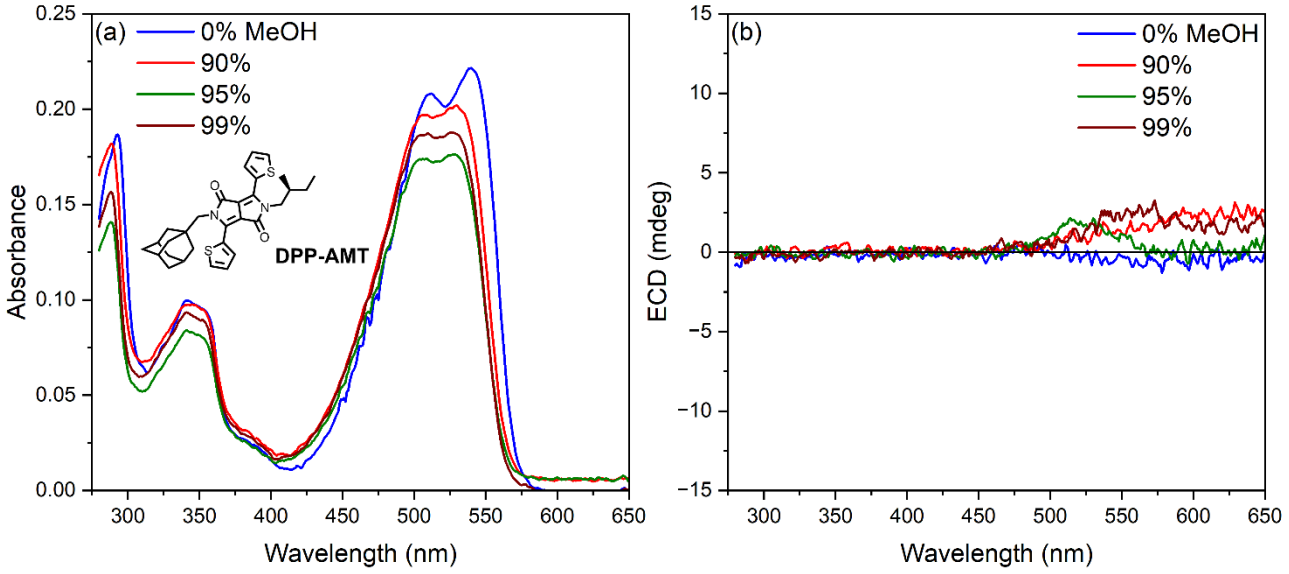

Figure S23.

Optical and chiroptical investigation of **DPP-AMT** dye **4** under condition of solution aggregation: (a) UV-Vis absorbance spectra and (b) ECD spectra in $CHCl_3$/MeOH mixtures with increasing amounts of MeOH (from 0% to 99%). Cell length 1 cm; sample concentration 10^{-5} M.

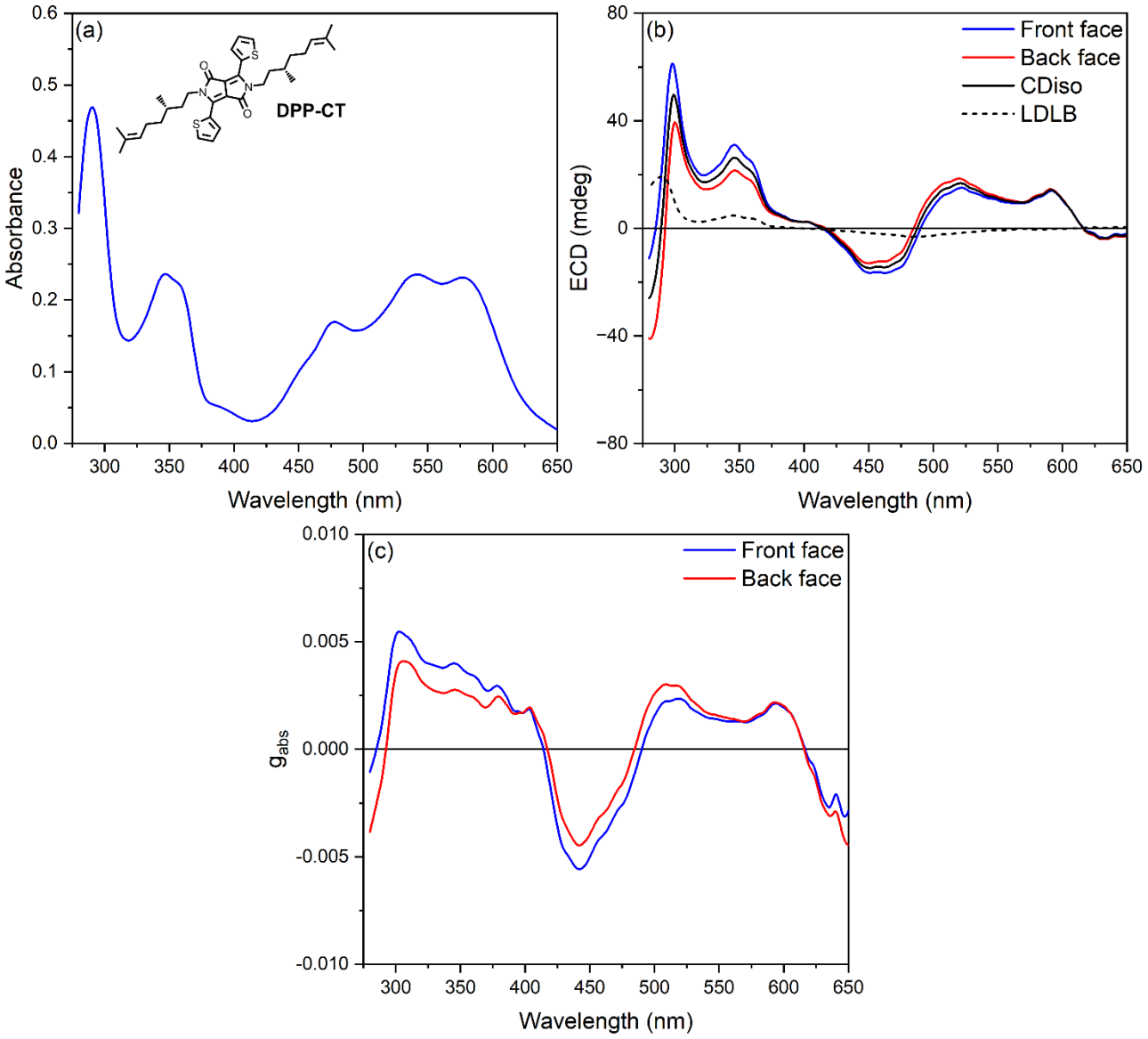

Figure S24.

Optical and chiroptical investigation for thin films of **DPP-CT** dye **1** prepared by spin-coating technique, before any annealing. (a) UV-Vis absorbance spectra. (b) ECD and (c) dissymmetry factor g_{abs} spectra recorded for the front face (blue line) and the back face (red line). For panel b: black continuous line is the front-back semi-sum of ECD, *i.e.*, calculated CDiso contribution; black dashed line is the front-back semi-difference of ECD, *i.e.*, calculated LDLB contribution.

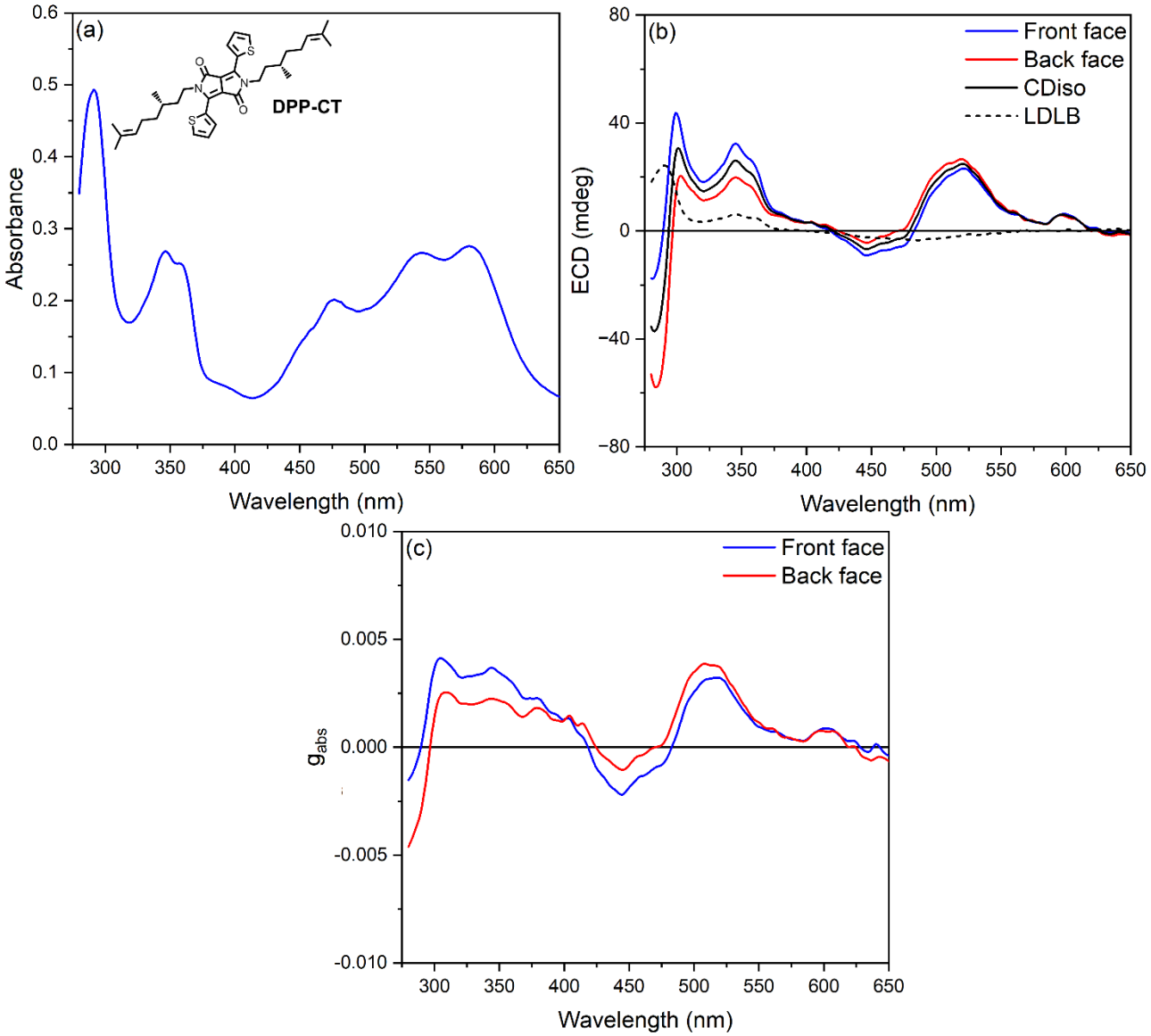

Figure S25.

Optical and chiroptical investigation for thin films of **DPP-CT** dye **1** prepared by spin-coating technique, after 10 min of solvent annealing under $CHCl_3$ vapours. (a) UV-Vis absorbance spectra. (b) ECD and (c) dissymmetry factor g_{abs} spectra recorded for the front face (blue line) and the back face (red line). For panel b: black continuous line is the front-back semi-sum of ECD, *i.e.*, calculated CDiso contribution; black dashed line is the front-back semi-difference of ECD, *i.e.*, calculated LDLB contribution.

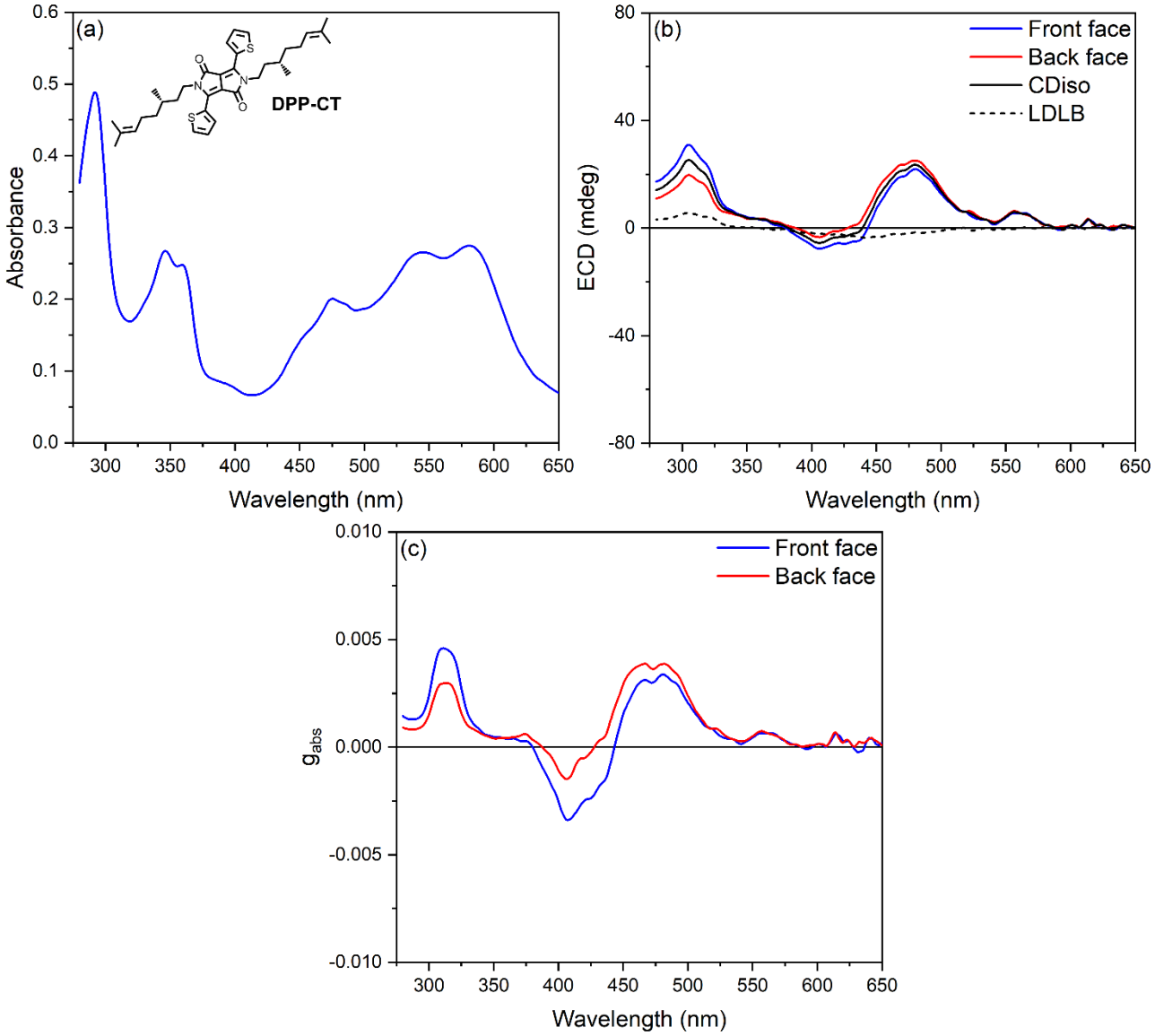

Figure S26.

Optical and chiroptical investigation for thin films of **DPP-CT** dye **1** prepared by spin-coating technique, after 20 min of solvent annealing under $CHCl_3$ vapours. (a) UV-Vis absorbance spectra. (b) ECD and (c) dissymmetry factor g_{abs} spectra recorded for the front face (blue line) and the back face (red line). For panel b: black continuous line is the front-back semi-sum of ECD, *i.e.*, calculated CDiso contribution; black dashed line is the front-back semi-difference of ECD, *i.e.*, calculated LDLB contribution.

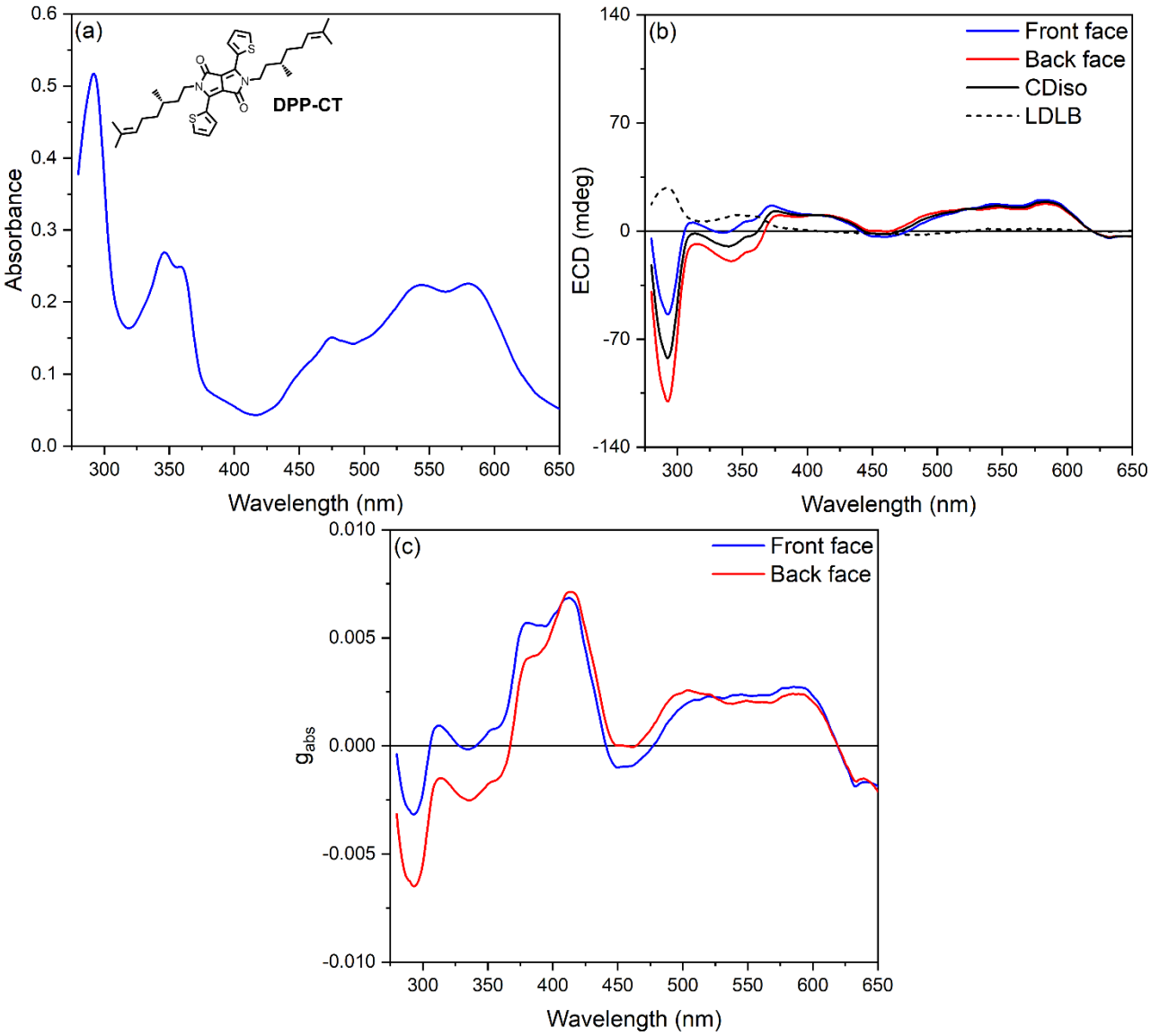

Figure S27.

Optical and chiroptical investigation for thin films of **DPP-CT** dye **1** prepared by spin-coating technique, after 40 min of solvent annealing under $CHCl_3$ vapours. (a) UV-Vis absorbance spectra. (b) ECD and (c) dissymmetry factor g_{abs} spectra recorded for the front face (blue line) and the back face (red line). For panel b: black continuous line is the front-back semi-sum of ECD, *i.e.*, calculated CDiso contribution; black dashed line is the front-back semi-difference of ECD, *i.e.*, calculated LDLB contribution.

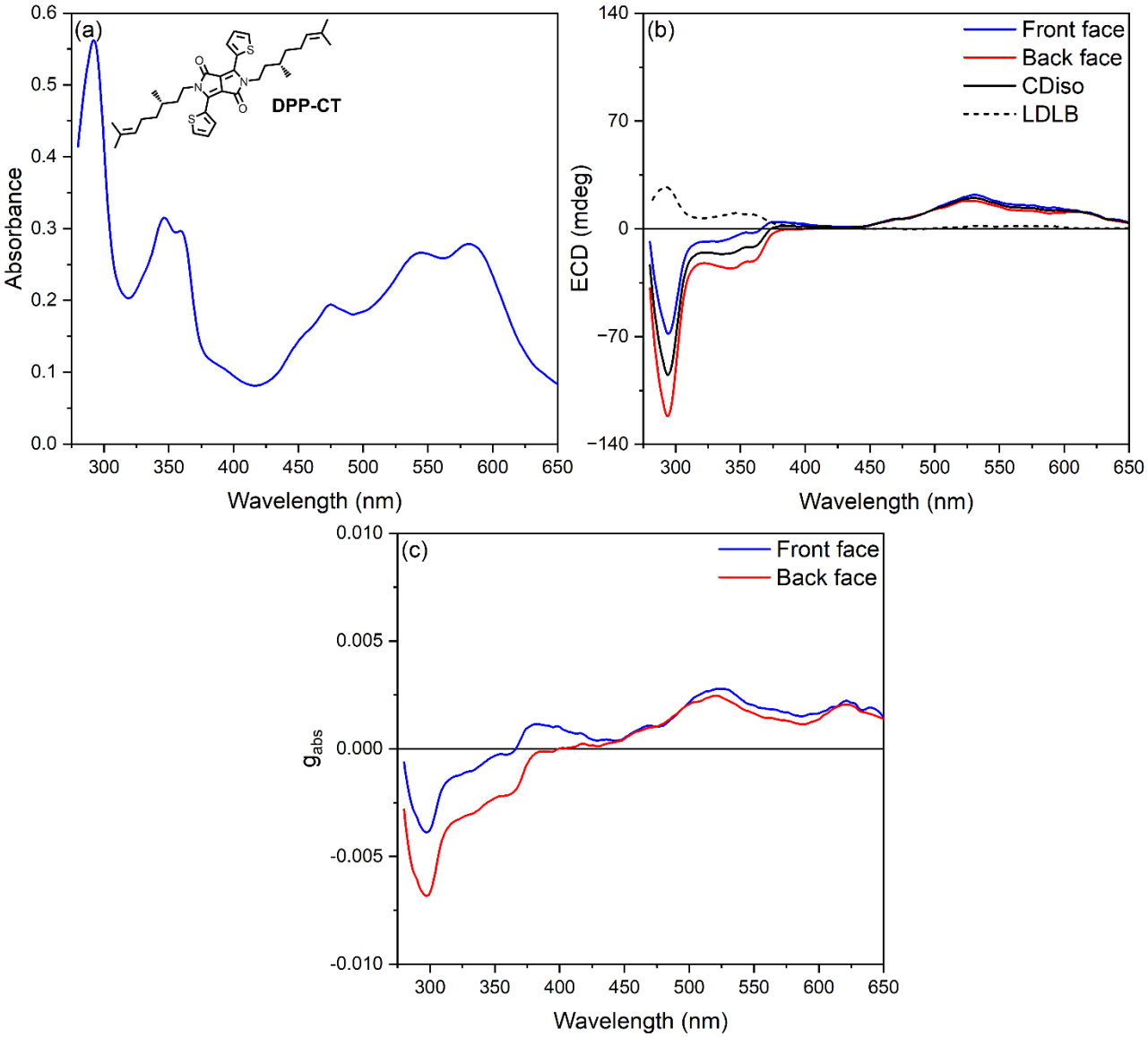

Figure S28.

Optical and chiroptical investigation for thin films of **DPP-CT** dye **1** prepared by spin-coating technique, after 1 h of thermal annealing at 110 °C. (a) UV-Vis absorbance spectra. (b) ECD and (c) dissymmetry factor g_{abs} spectra recorded for the front face (blue line) and the back face (red line). For panel b: black continuous line is the front-back semi-sum of ECD, *i.e.*, calculated CDiso contribution; black dashed line is the front-back semi-difference of ECD, *i.e.*, calculated LDLB contribution.

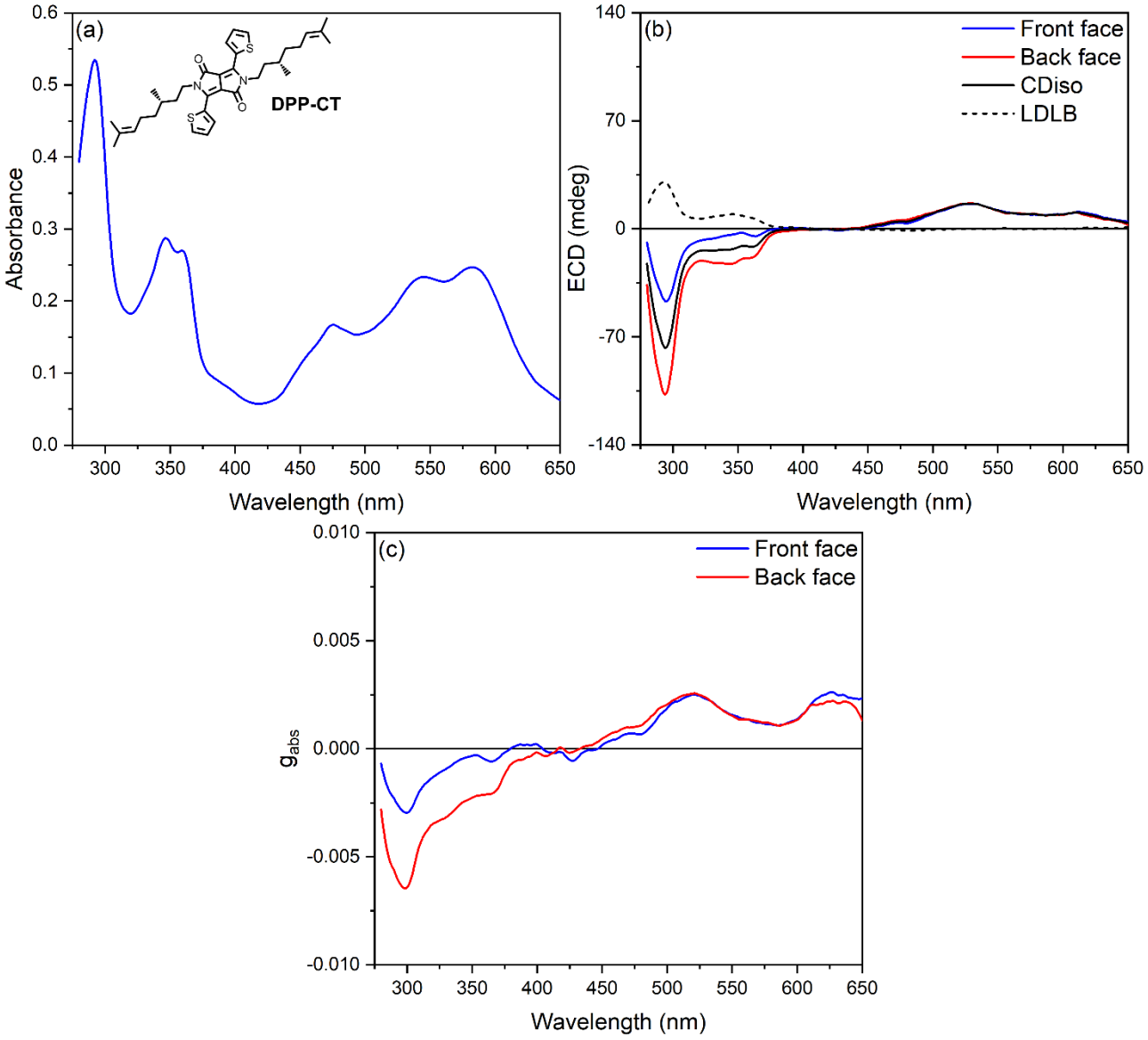

Figure S29.

Optical and chiroptical investigation for thin films of **DPP-CT** dye **1** prepared by spin-coating technique, after 2 h of thermal annealing at 110 °C. (a) UV-Vis absorbance spectra. (b) ECD and (c) dissymmetry factor g_{abs} spectra recorded for the front face (blue line) and the back face (red line). For panel b: black continuous line is the front-back semi-sum of ECD, *i.e.*, calculated CDiso contribution; black dashed line is the front-back semi-difference of ECD, *i.e.*, calculated LDLB contribution.

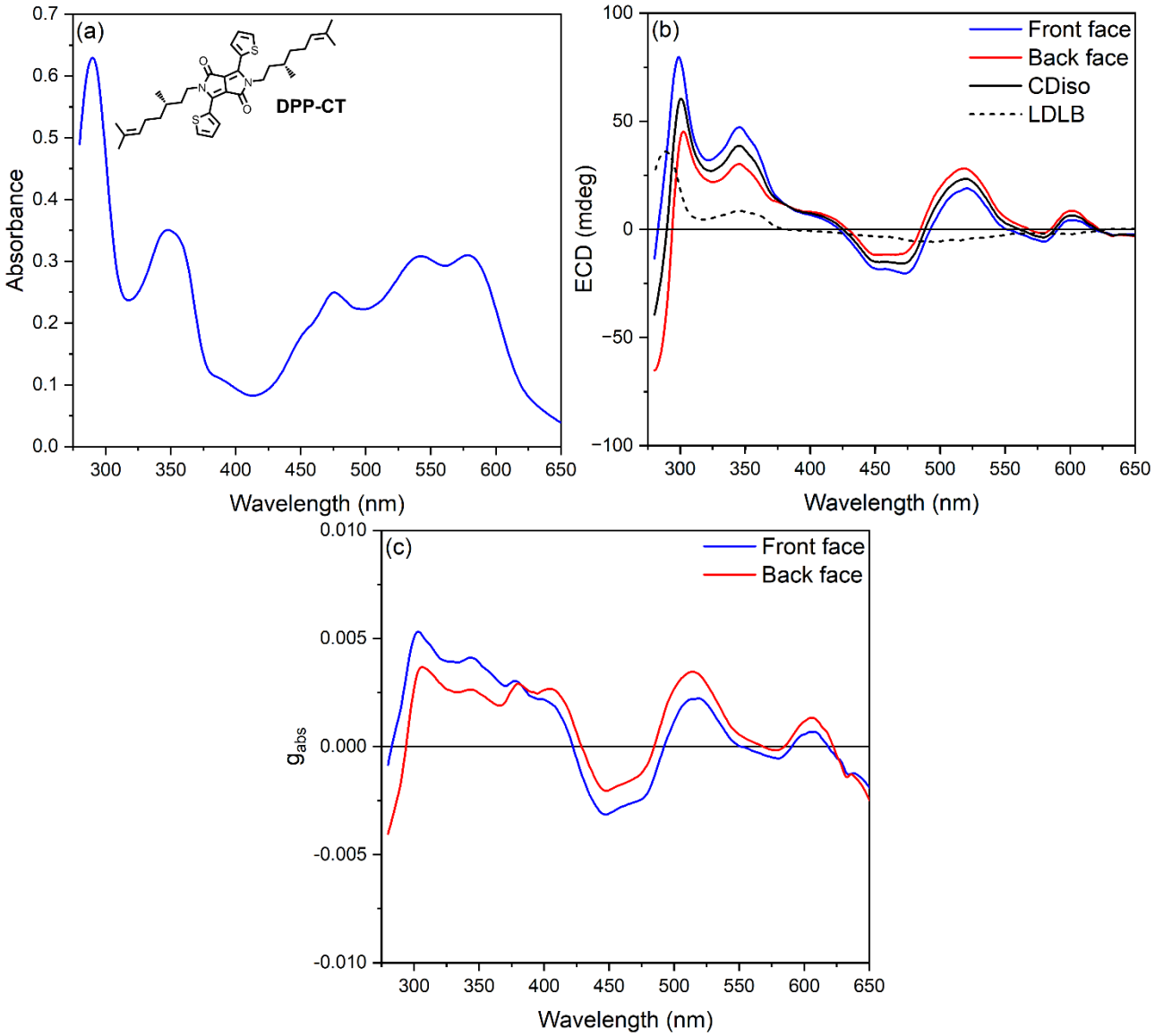

Figure S30.

Optical and chiroptical investigation for thin films of **DPP-CT** dye **1** prepared by spin-coating technique, after 1 month of ageing. (a) UV-Vis absorbance spectra. (b) ECD and (c) dissymmetry factor g_{abs} spectra recorded for the front face (blue line) and the back face (red line). For panel b: black continuous line is the front-back semi-sum of ECD, *i.e.*, calculated CDiso contribution; black dashed line is the front-back semi-difference of ECD, *i.e.*, calculated LDLB contribution.

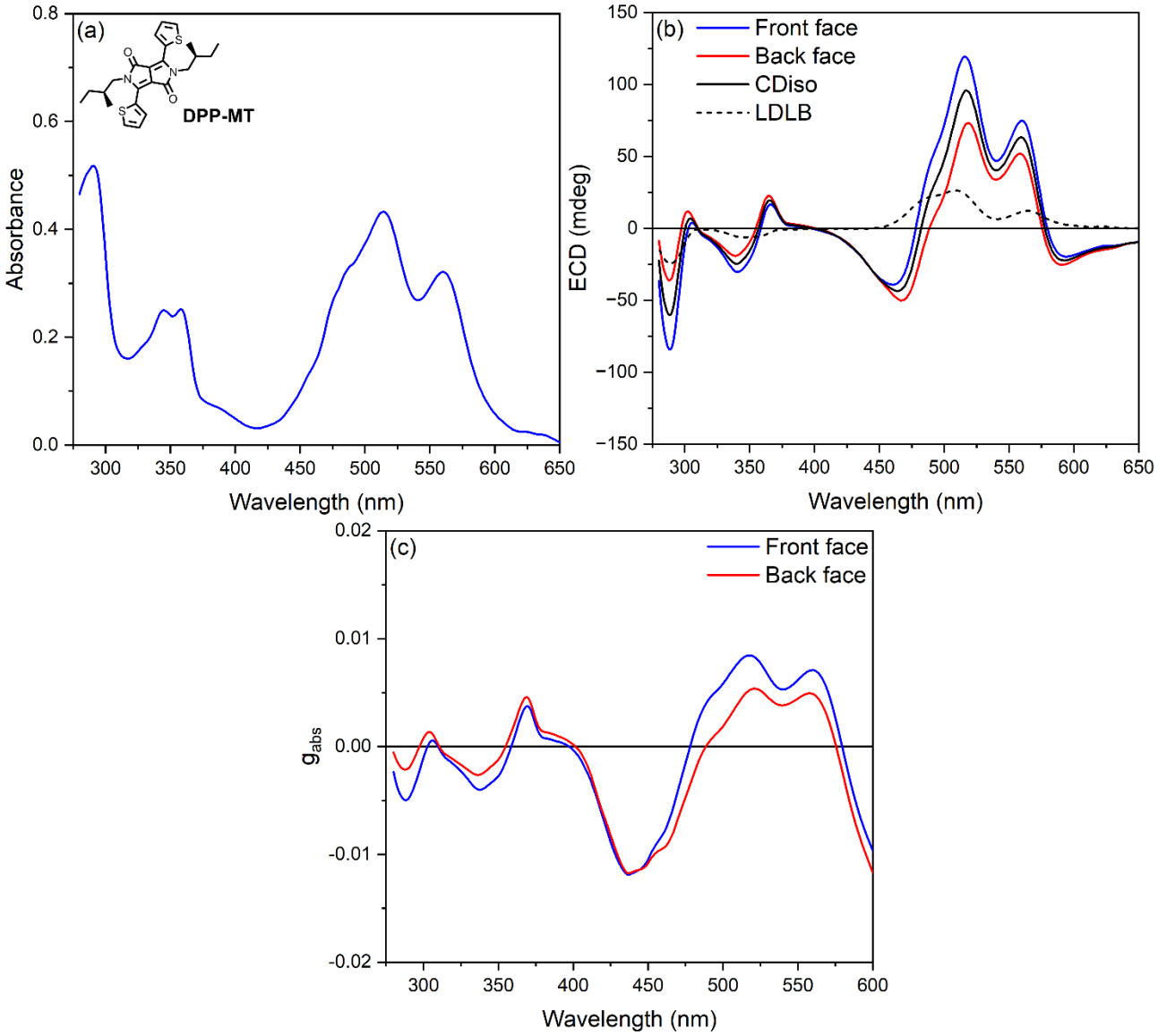

Figure S31.

Optical and chiroptical investigation for thin films of **DPP-MT** dye **2** prepared by spin-coating technique, before any annealing. (a) UV-Vis absorbance spectra. (b) ECD and (c) dissymmetry factor g_{abs} spectra recorded for the front face (blue line) and the back face (red line). For panel b: black continuous line is the front-back semi-sum of ECD, *i.e.*, calculated CDiso contribution; black dashed line is the front-back semi-difference of ECD, *i.e.*, calculated LDLB contribution.

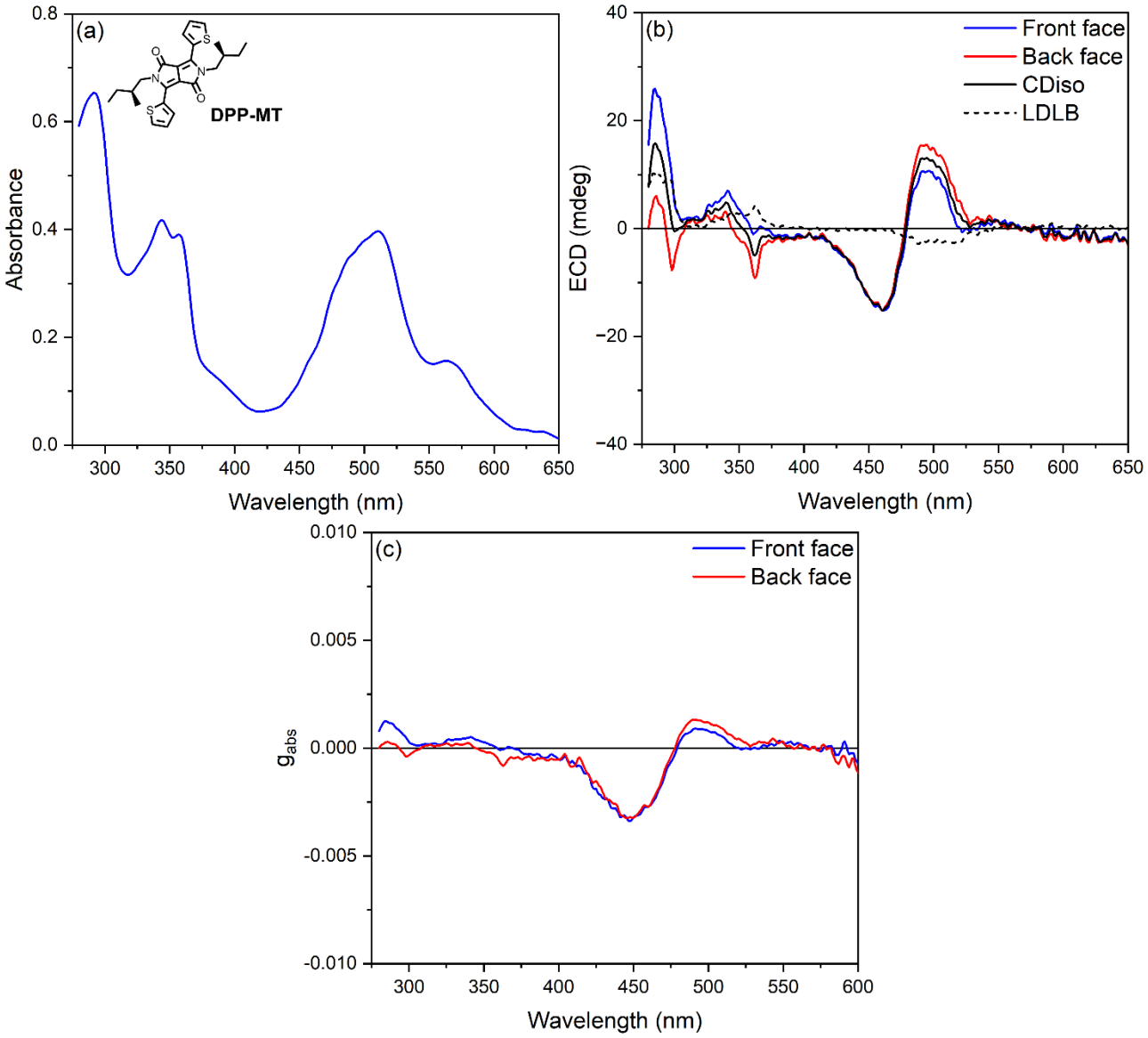

Figure S32.

Optical and chiroptical investigation for thin films of **DPP-MT** dye **2** prepared by spin-coating technique, after 10 min of solvent annealing under $CHCl_3$ vapours. (a) UV-Vis absorbance spectra. (b) ECD and (c) dissymmetry factor g_{abs} spectra recorded for the front face (blue line) and the back face (red line). For panel b: black continuous line is the front-back semi-sum of ECD, *i.e.*, calculated CDiso contribution; black dashed line is the front-back semi-difference of ECD, *i.e.*, calculated LDLB contribution.

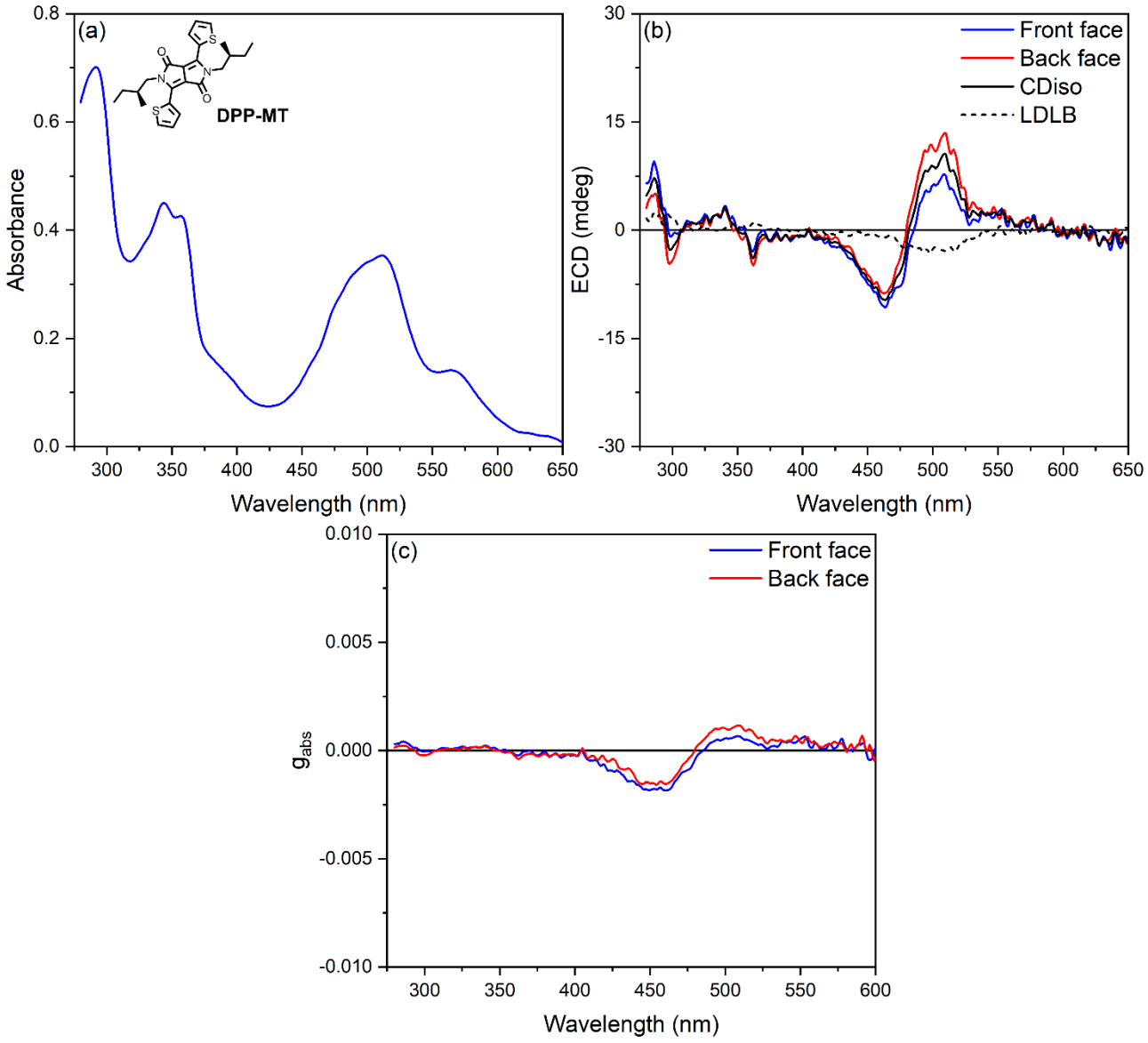

Figure S33.

Optical and chiroptical investigation for thin films of **DPP-MT** dye **2** prepared by spin-coating technique, after 20 min of solvent annealing under $CHCl_3$ vapours. (a) UV-Vis absorbance spectra. (b) ECD and (c) dissymmetry factor g_{abs} spectra recorded for the front face (blue line) and the back face (red line). For panel b: black continuous line is the front-back semi-sum of ECD, *i.e.*, calculated CDiso contribution; black dashed line is the front-back semi-difference of ECD, *i.e.*, calculated LDLB contribution.

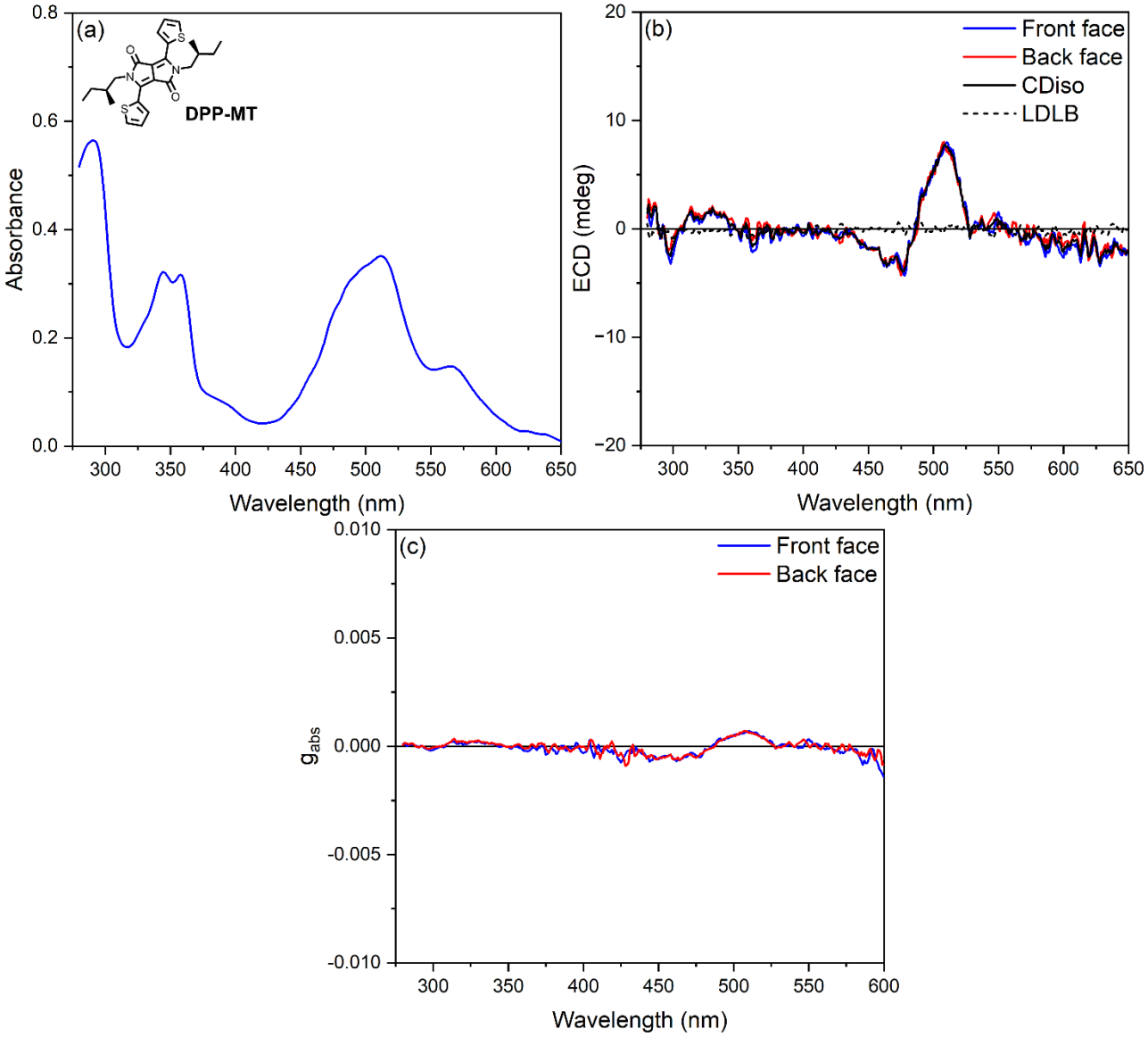

Figure S34.

Optical and chiroptical investigation for thin films of **DPP-MT** dye **2** prepared by spin-coating technique, after 1 h of thermal annealing at 170 °C. (a) UV-Vis absorbance spectra. (b) ECD and (c) dissymmetry factor g_{abs} spectra recorded for the front face (blue line) and the back face (red line). For panel b: black continuous line is the front-back semi-sum of ECD, *i.e.*, calculated CDiso contribution; black dashed line is the front-back semi-difference of ECD, *i.e.*, calculated LDLB contribution.

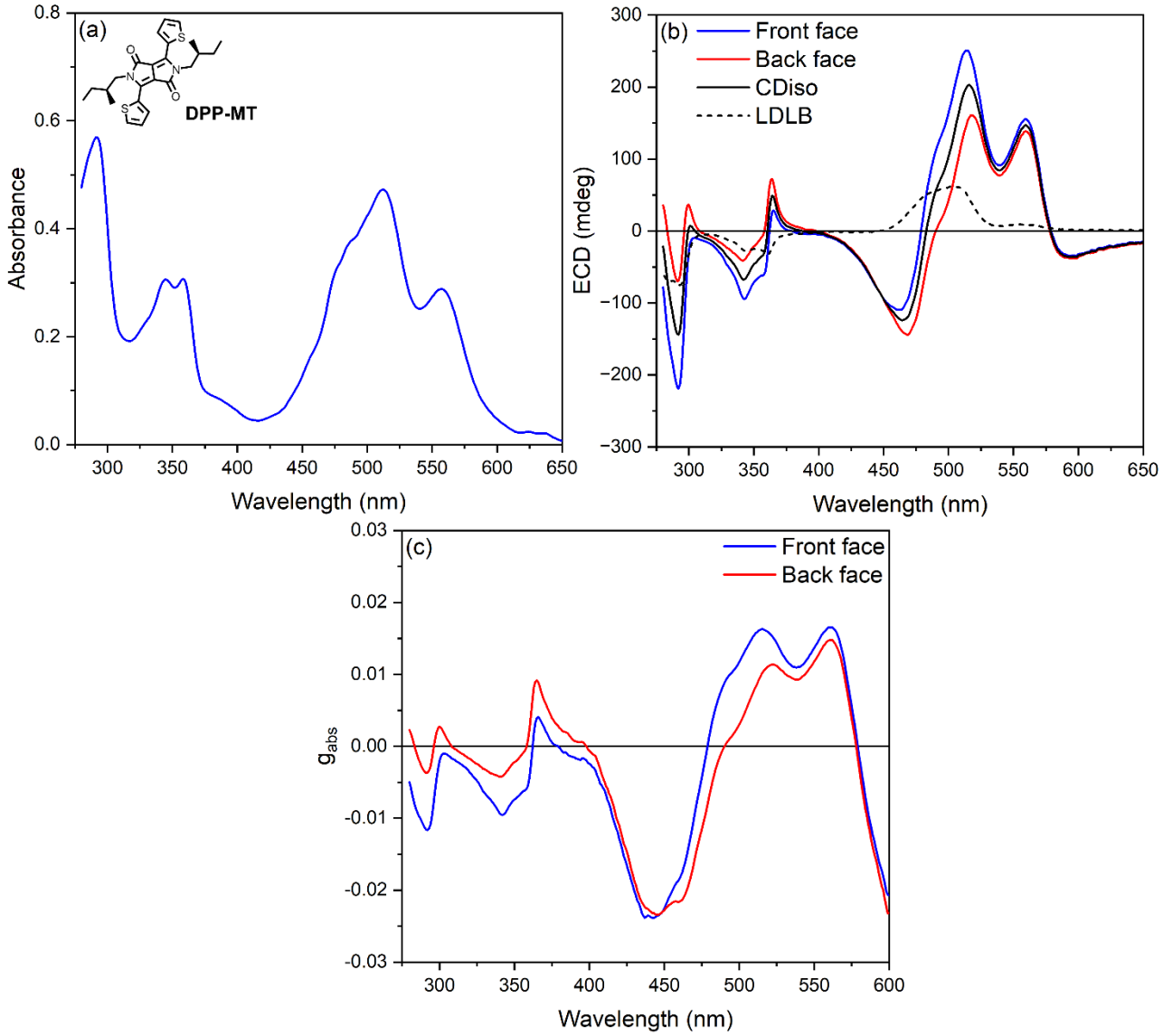

Figure S35.

Optical and chiroptical investigation for thin films of **DPP-MT** dye **2** prepared by spin-coating technique, after 1 month of ageing. (a) UV-Vis absorbance spectra. (b) ECD and (c) dissymmetry factor g_{abs} spectra recorded for the front face (blue line) and the back face (red line). For panel b: black continuous line is the front-back semi-sum of ECD, *i.e.*, calculated CDiso contribution; black dashed line is the front-back semi-difference of ECD, *i.e.*, calculated LDLB contribution.

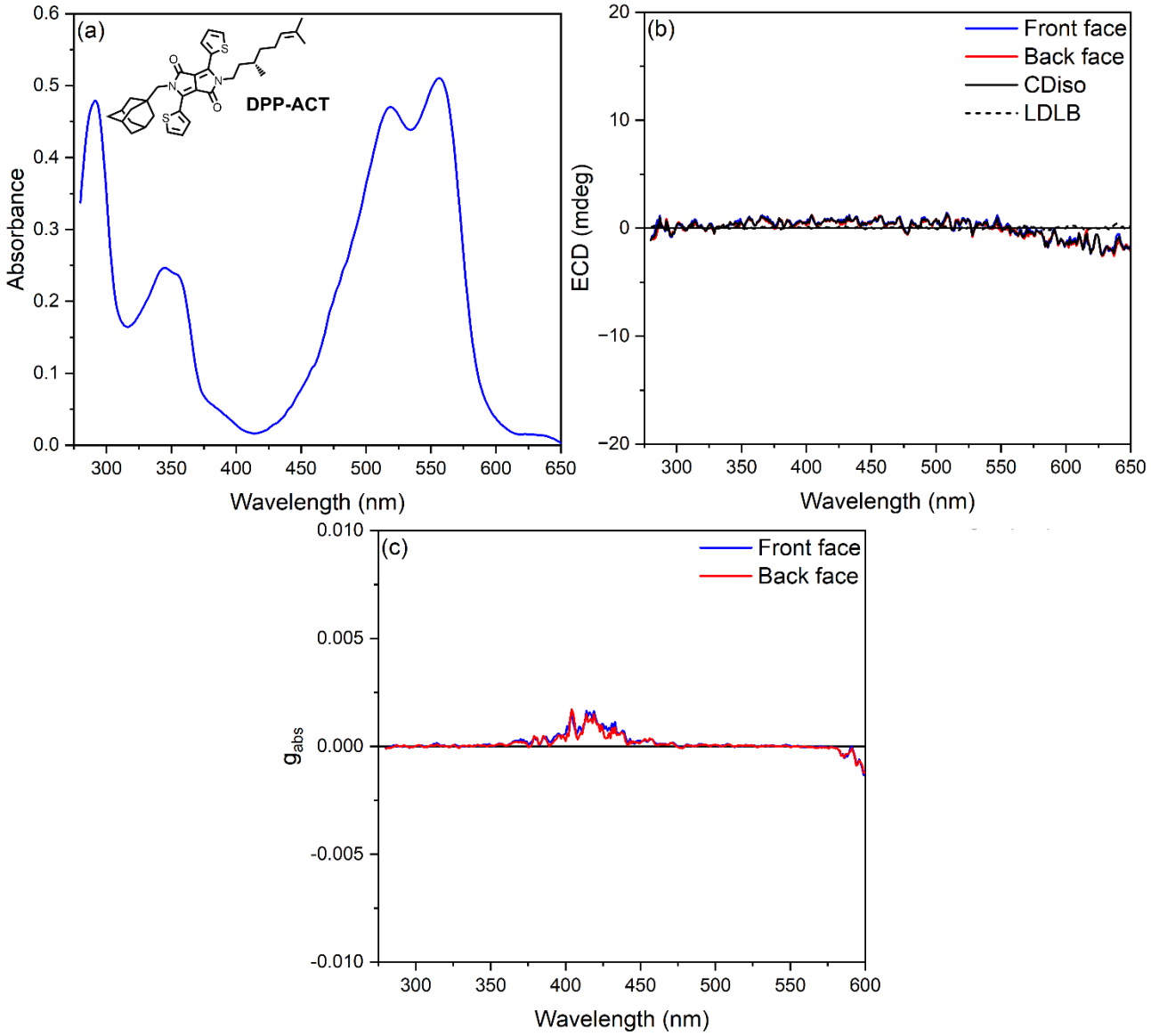

Figure S36.

Optical and chiroptical investigation for thin films of **DPP-ACT** dye **3** prepared by spin-coating technique, before any annealing. (a) UV-Vis absorbance spectra. (b) ECD and (c) dissymmetry factor g_{abs} spectra recorded for the front face (blue line) and the back face (red line). For panel b: black continuous line is the front-back semi-sum of ECD, *i.e.*, calculated CDiso contribution; black dashed line is the front-back semi-difference of ECD, *i.e.*, calculated LDLB contribution.

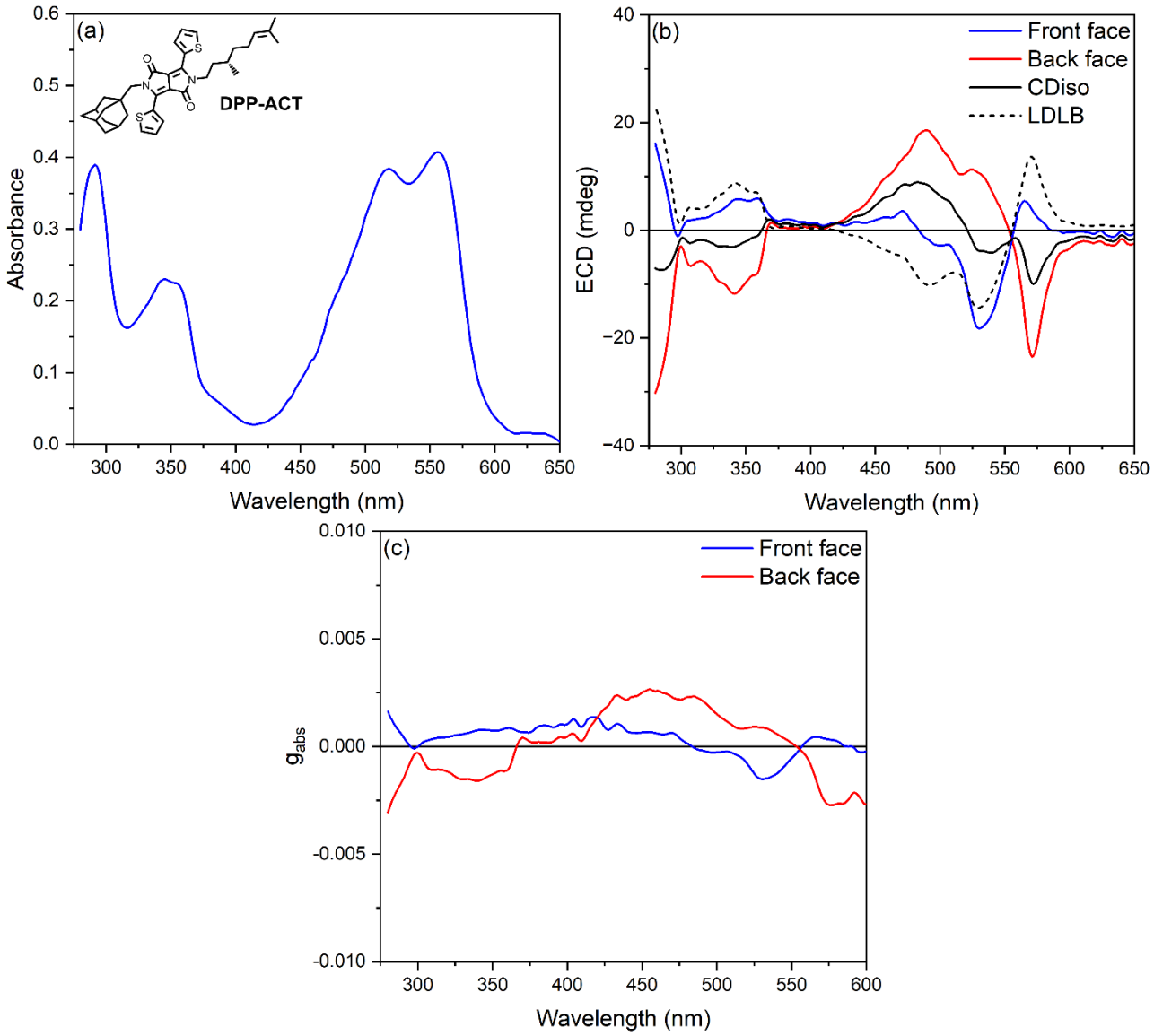

Figure S37.

Optical and chiroptical investigation for thin films of **DPP-ACT** dye **3** prepared by spin-coating technique, after 30 min of thermal annealing at 110 °C. (a) UV-Vis absorbance spectra. (b) ECD and (c) dissymmetry factor g_{abs} spectra recorded for the front face (blue line) and the back face (red line). For panel b: black continuous line is the front-back semi-sum of ECD, *i.e.*, calculated CDiso contribution; black dashed line is the front-back semi-difference of ECD, *i.e.*, calculated LDLB contribution.

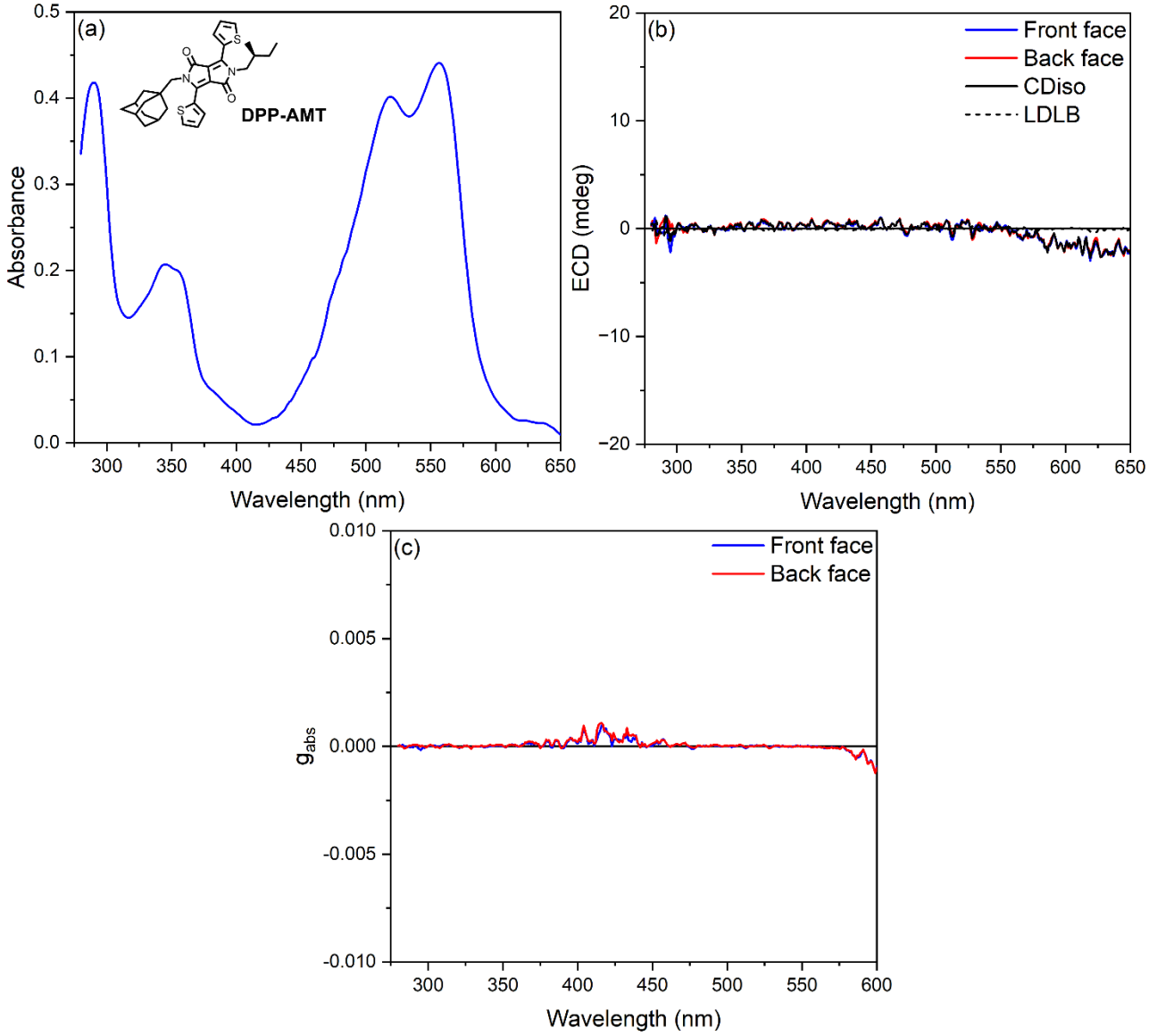

Figure S38.

Optical and chiroptical investigation for thin films of **DPP-AMT** dye **4** prepared by spin-coating technique, before any annealing. (a) UV-Vis absorbance spectra. (b) ECD and (c) dissymmetry factor g_{abs} spectra recorded for the front face (blue line) and the back face (red line). For panel b: black continuous line is the front-back semi-sum of ECD, *i.e.*, calculated CDiso contribution; black dashed line is the front-back semi-difference of ECD, *i.e.*, calculated LDLB contribution.

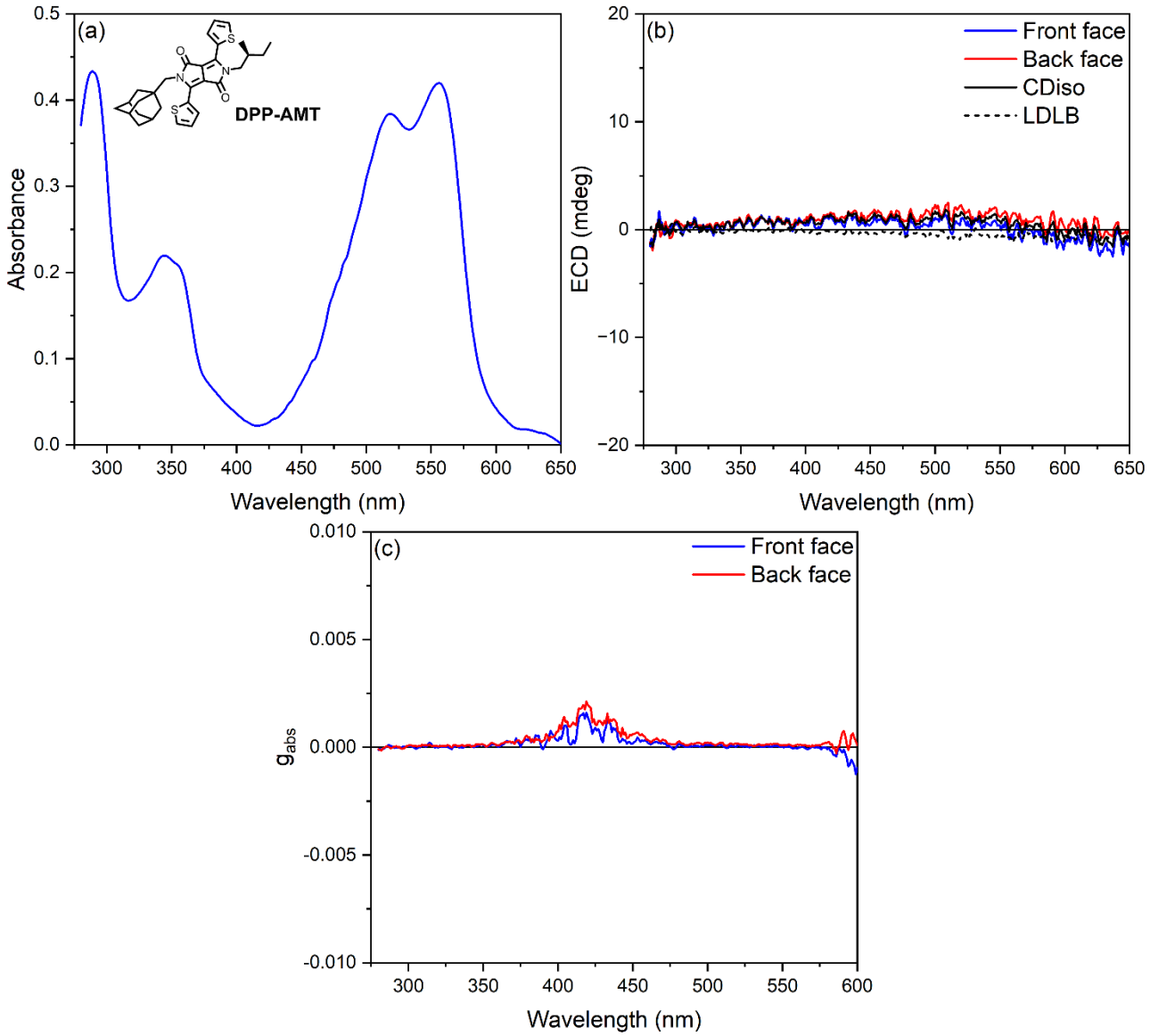

Figure S39.

Optical and chiroptical investigation for thin films of **DPP-AMT** dye **4** prepared by spin-coating technique, after 1 h of thermal annealing at 120 °C. (a) UV-Vis absorbance spectra. (b) ECD and (c) dissymmetry factor g_{abs} spectra recorded for the front face (blue line) and the back face (red line). For panel b: black continuous line is the front-back semi-sum of ECD, *i.e.*, calculated CDiso contribution; black dashed line is the front-back semi-difference of ECD, *i.e.*, calculated LDLB contribution.

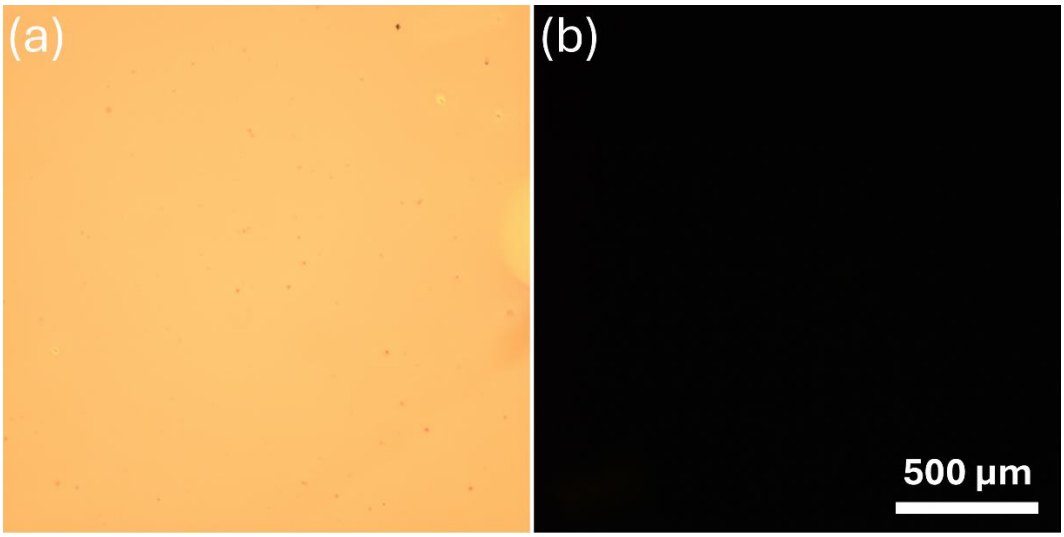

Figure S40.

Optical microscopy investigation for thin films of **DPP-CT** dye **1** prepared by spin-coating technique, before any annealing. Images recorded: (a) in bright field; (b) under cross-polarized filters.

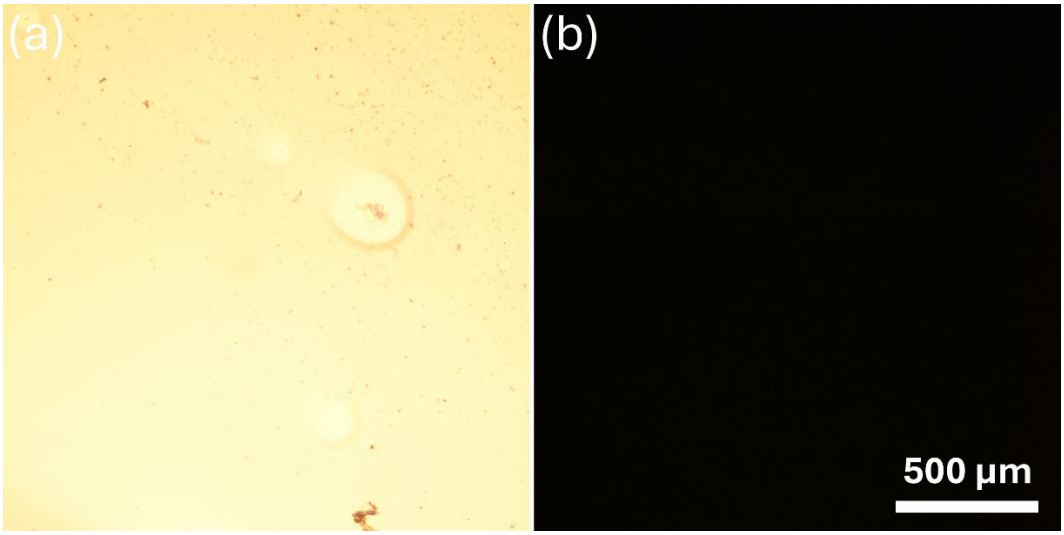

Figure S41.

Optical microscopy investigation for thin films of **DPP-CT** dye **1** prepared by spin-coating technique, after 40 min of solvent annealing under $CHCl_3$ vapours. Images recorded: (a) in bright field; (b) under cross-polarized filters.

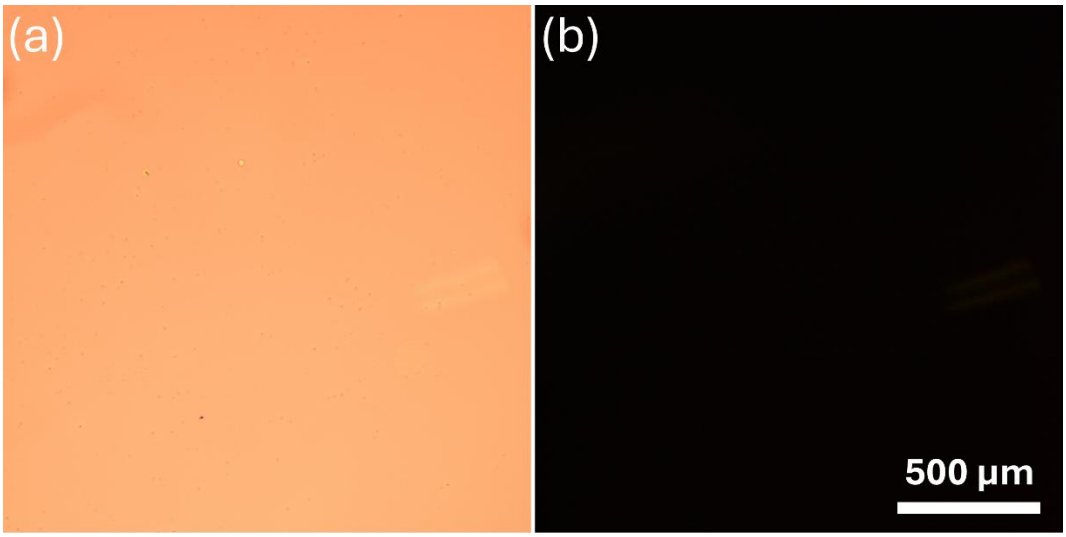

Figure S42.

Optical microscopy investigation for thin films of **DPP-MT** dye **2** prepared by spin-coating technique, before any annealing. Images recorded: (a) in bright field; (b) under cross-polarized filters.

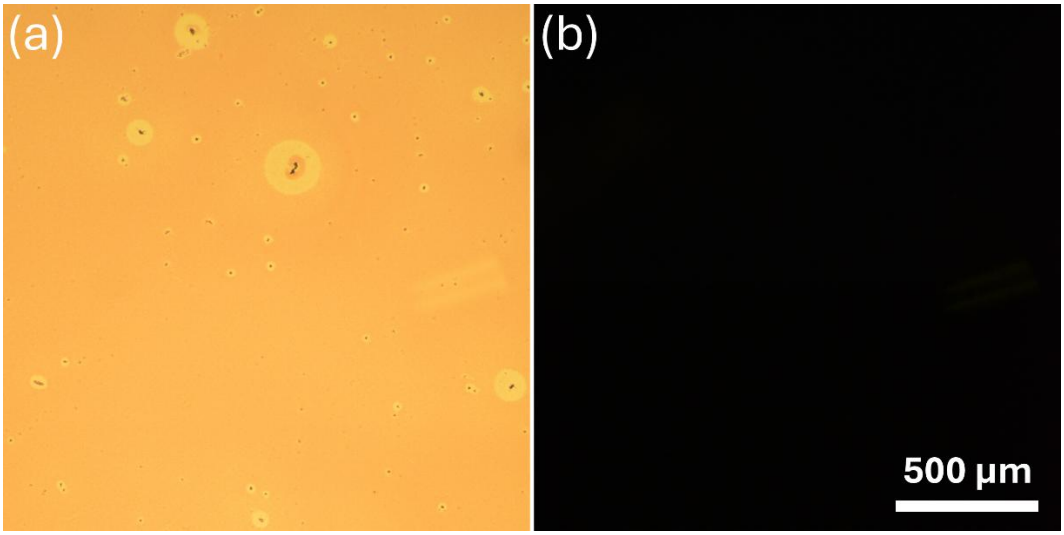

Figure S43.

Optical microscopy investigation for thin films of **DPP-MT** dye **2** prepared by spin-coating technique, after 10 min of solvent annealing under $CHCl_3$ vapours. Images recorded: (a) in bright field; (b) under cross-polarized filters.

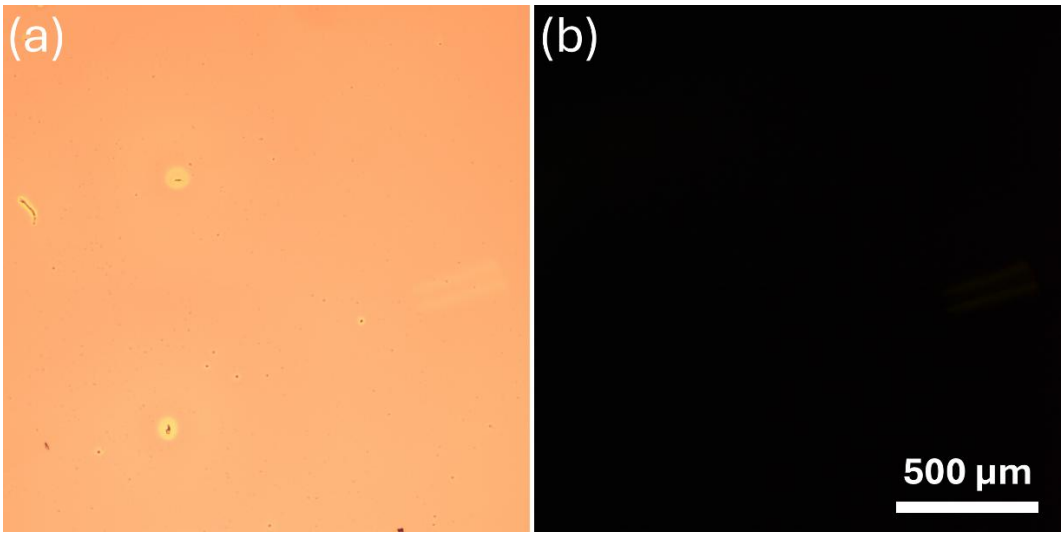

Figure S44.

Optical microscopy investigation for thin films of **DPP-ACT** dye **3** prepared by spin-coating technique, before any annealing. Images recorded: (a) in bright field; (b) under cross-polarized filters.

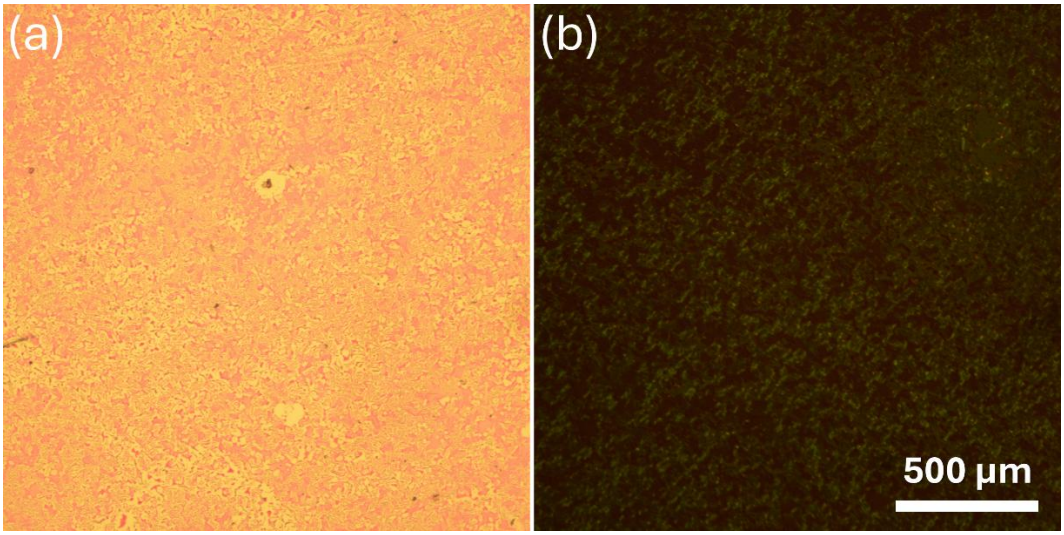

Figure S45.

Optical microscopy investigation for thin films of **DPP-ACT** dye **3** prepared by spin-coating technique, after 30 min of thermal annealing at 110 °C. Images recorded: (a) in bright field; (b) under cross-polarized filters.

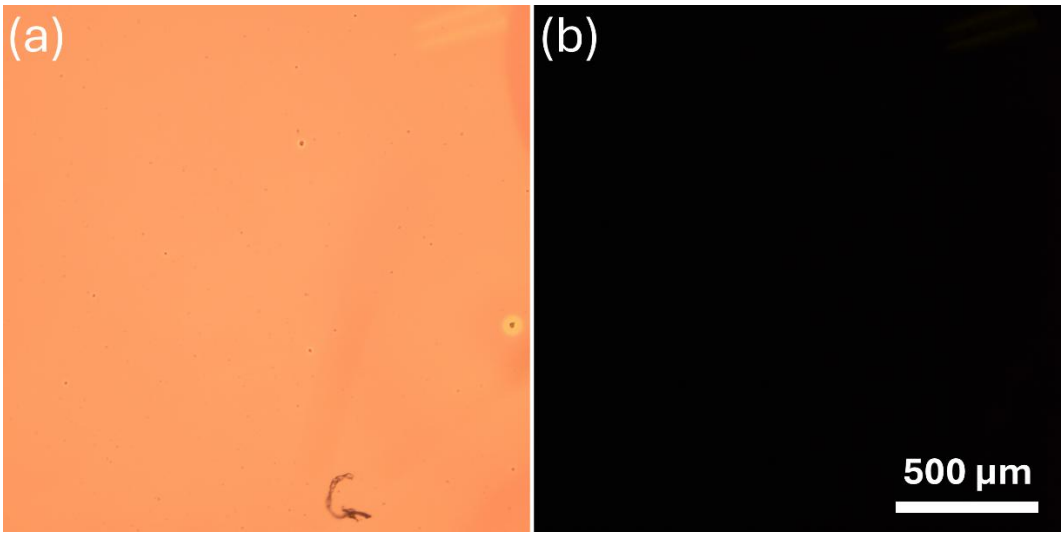

Figure S46.

Optical microscopy investigation for thin films of **DPP-AMT** dye **4** prepared by spin-coating technique, before any annealing. Images recorded: (a) in bright field; (b) under cross-polarized filters.

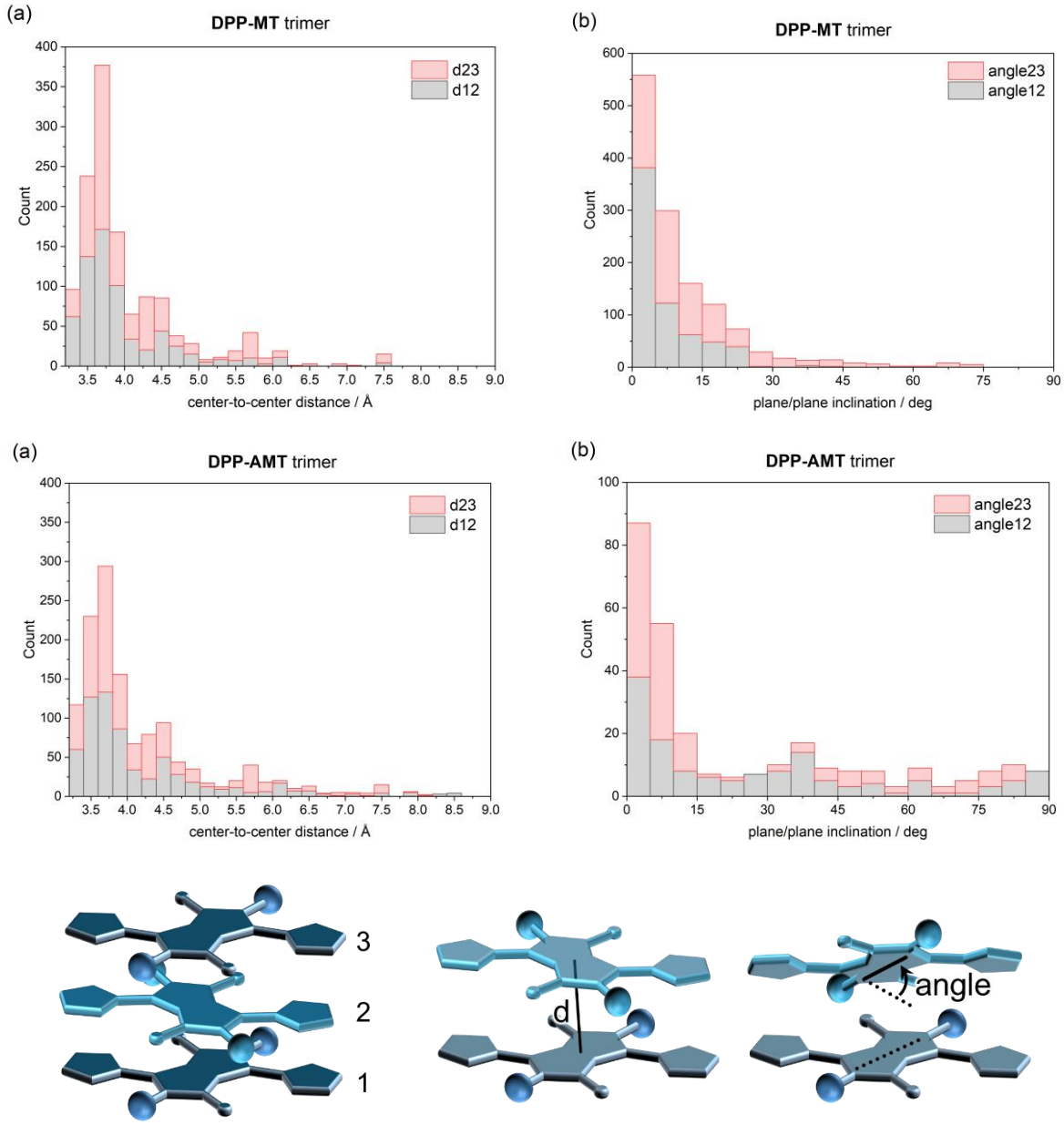

Figure S47.

Analysis of CREST results for the trimers of **DPP-MT (2)** (top row) and **DPP-AMT (4)** (middle row). The distribution of distances between DPP ring centres (panels (a)) and angles of inclination between average DPP planes (panels (b)) is shown. The bottom row displays the numbering used in the labels and the definition of distance and angle of inclination.

^{1}H-NMR Spectra of Intermediates

1-(Bromomethyl)adamantane (5):

^{1}H-NMR (80 MHz, $CDCl_3$)

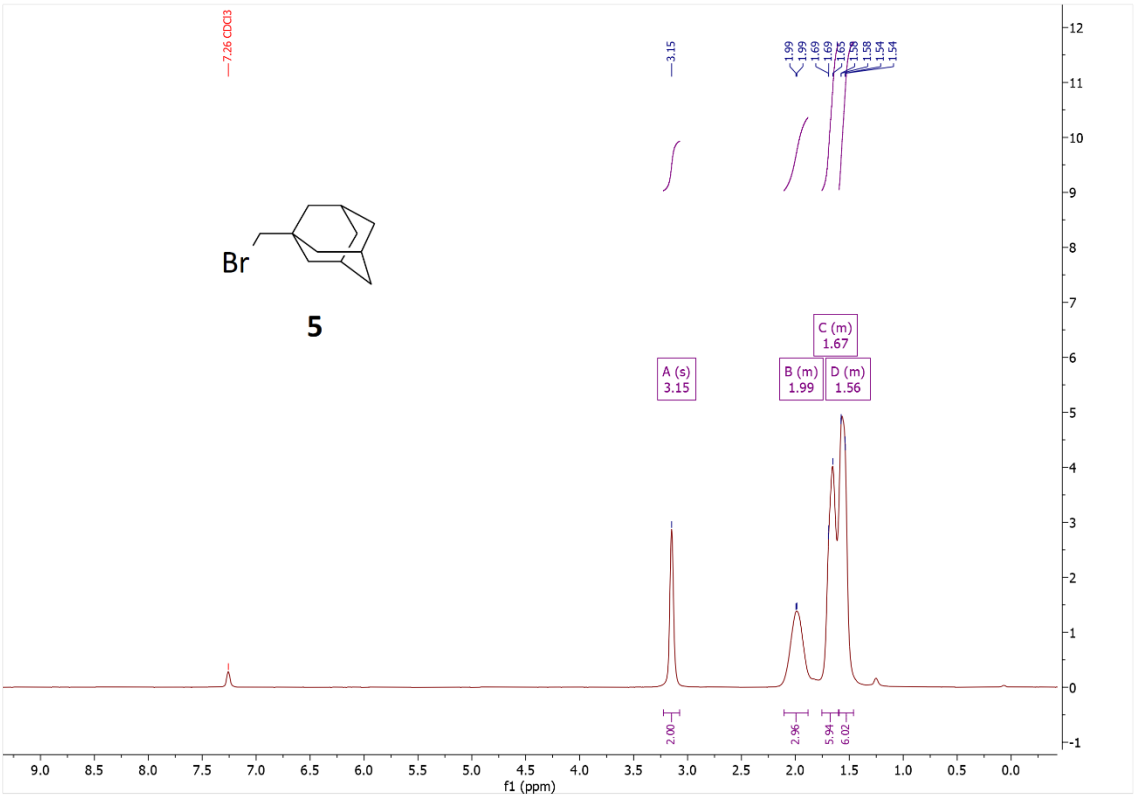

(*S*)-3,7-Dimethyloct-6-en-1-yl 4-methylbenzenesulfonate (6):

^{1}H-NMR (80 MHz, $CDCl_3$)

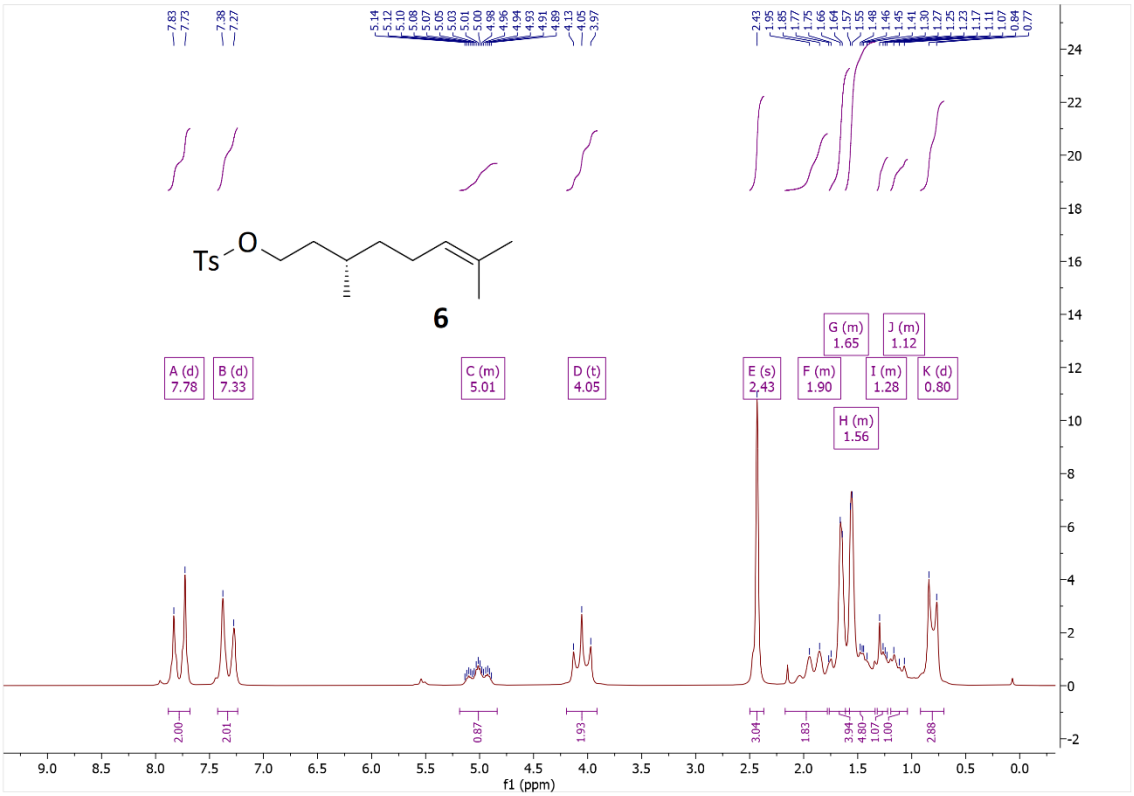

(*S*)-2-Methylbutyl 4-methylbenzenesulfonate (7):

^{1}H-NMR (80 MHz, $CDCl_3$)

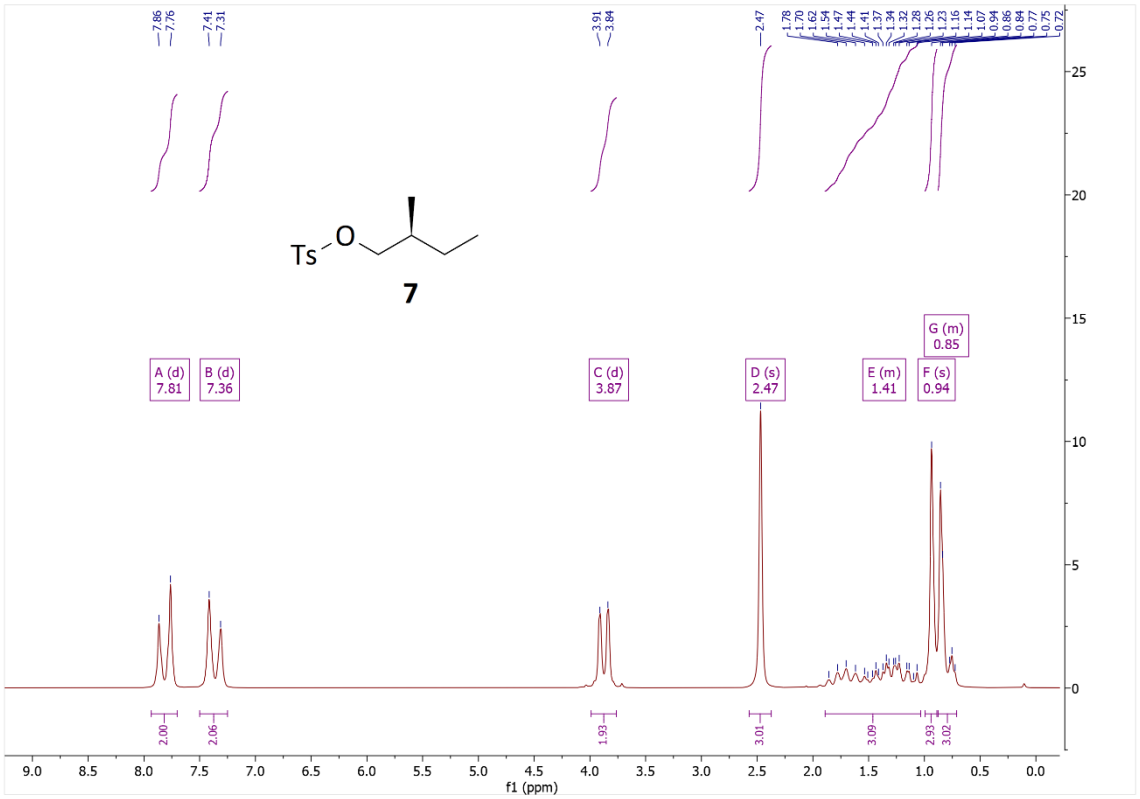

2-(Adamantan-1-yl)methyl-3,6-di(thiophen-2-yl)-2,5-dihydropyrrolo[3,4-*c*]pyrrole-1,4-dione (9):

^{1}H-NMR (500 MHz, $CDCl_3$)

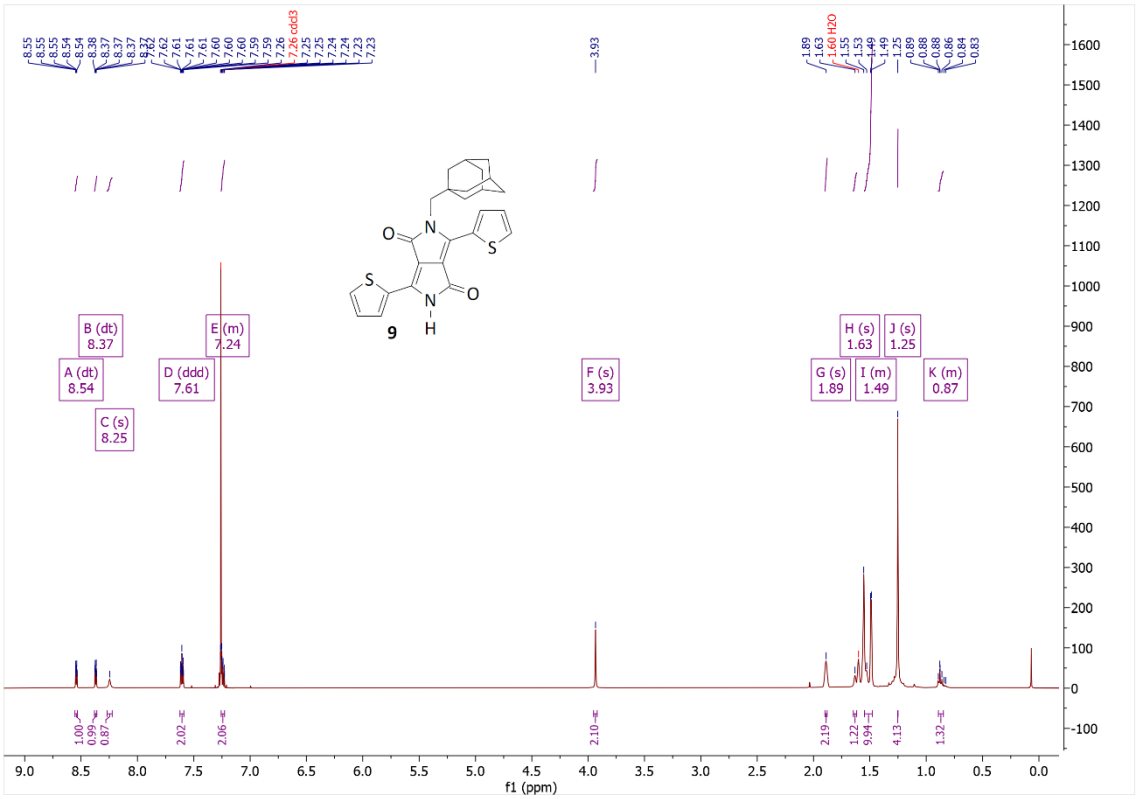

^{1}H-NMR and ^{13}C-NMR Spectra of Final Products

2,5-Bis((*S*)-3,7-dimethyloct-6-en-1-yl)-3,6-di(thiophen-2-yl)-2,5-dihydropyrrolo[3,4-*c*]pyrrole-1,4-dione (DPP-CT, 1):

^{1}H-NMR (500 MHz, $CDCl_3$)

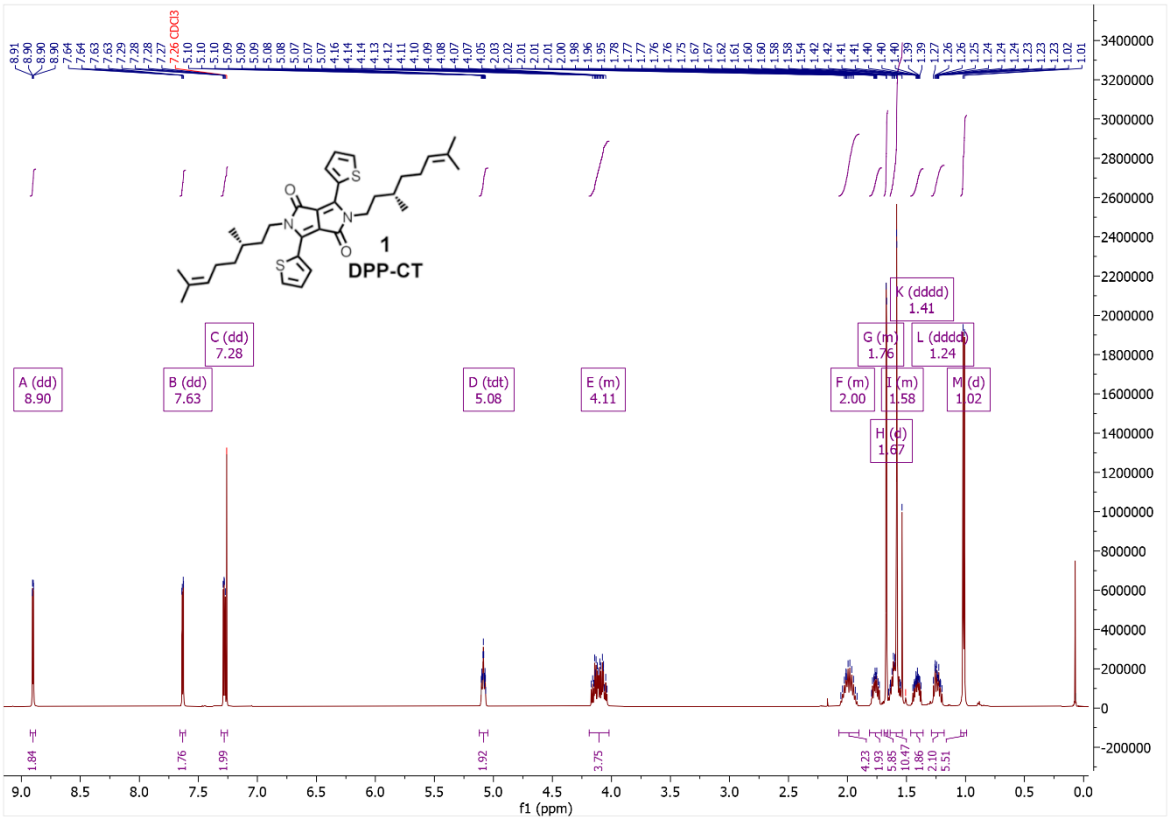

^{13}C-NMR (126 MHz, $CDCl_3$)

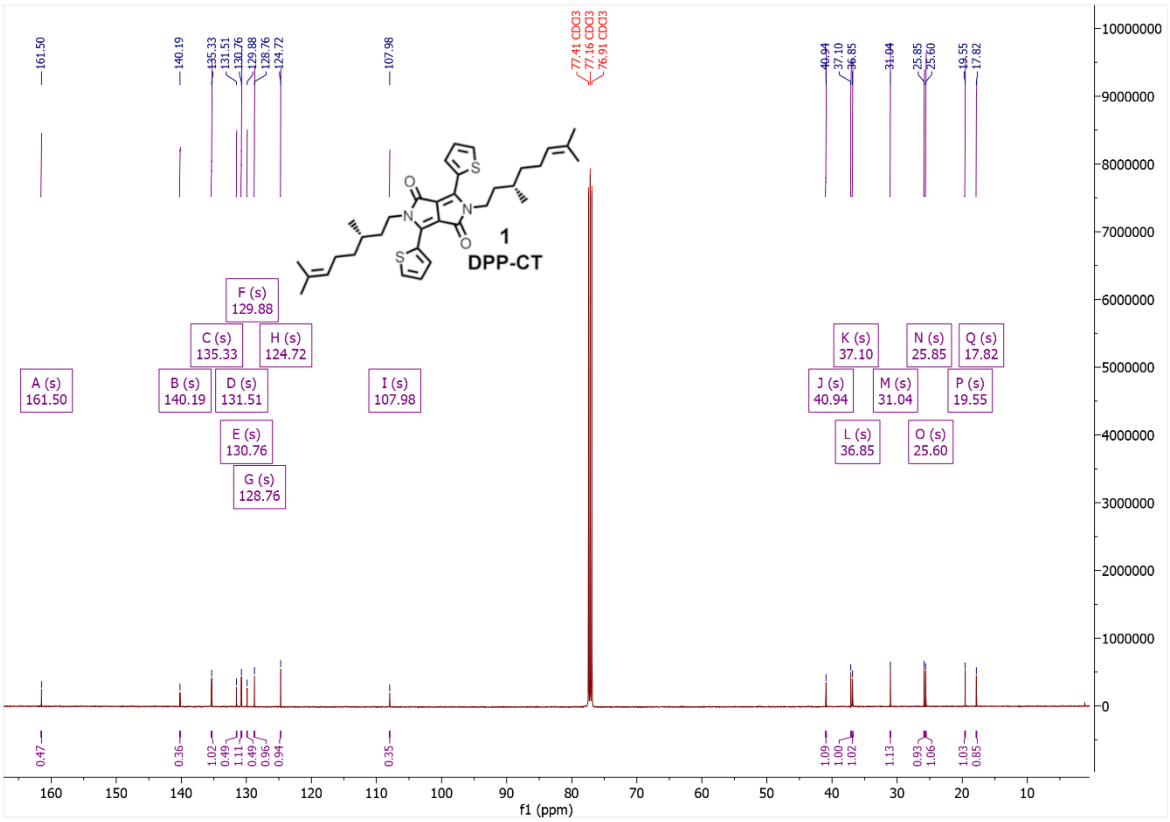

2,5-Bis((*S*)-2-methylbutyl)-3,6-di(thiophen-2-yl)-2,5-dihydropyrrolo[3,4-*c*]pyrrole-1,4-dione (DPP-MT, 2):

^{1}H-NMR (500 MHz, $CDCl_3$)

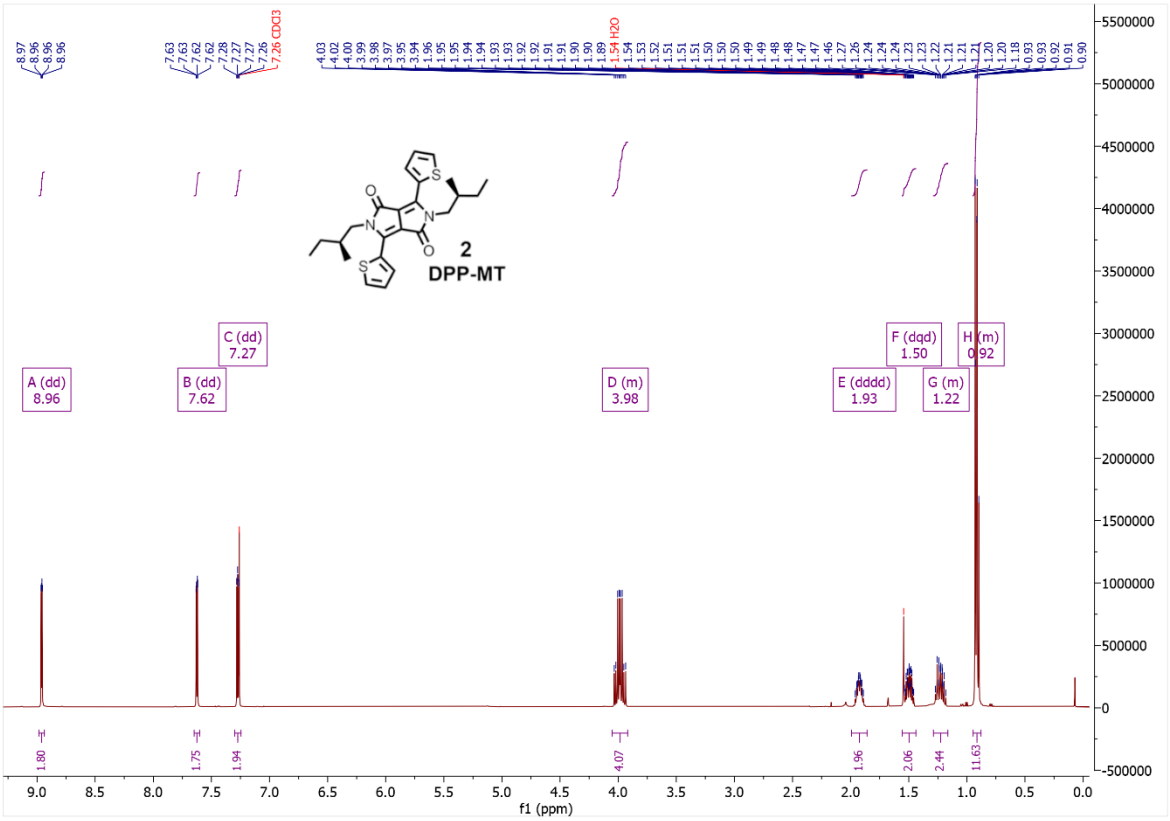

^{13}C-NMR (126 MHz, $CDCl_3$)

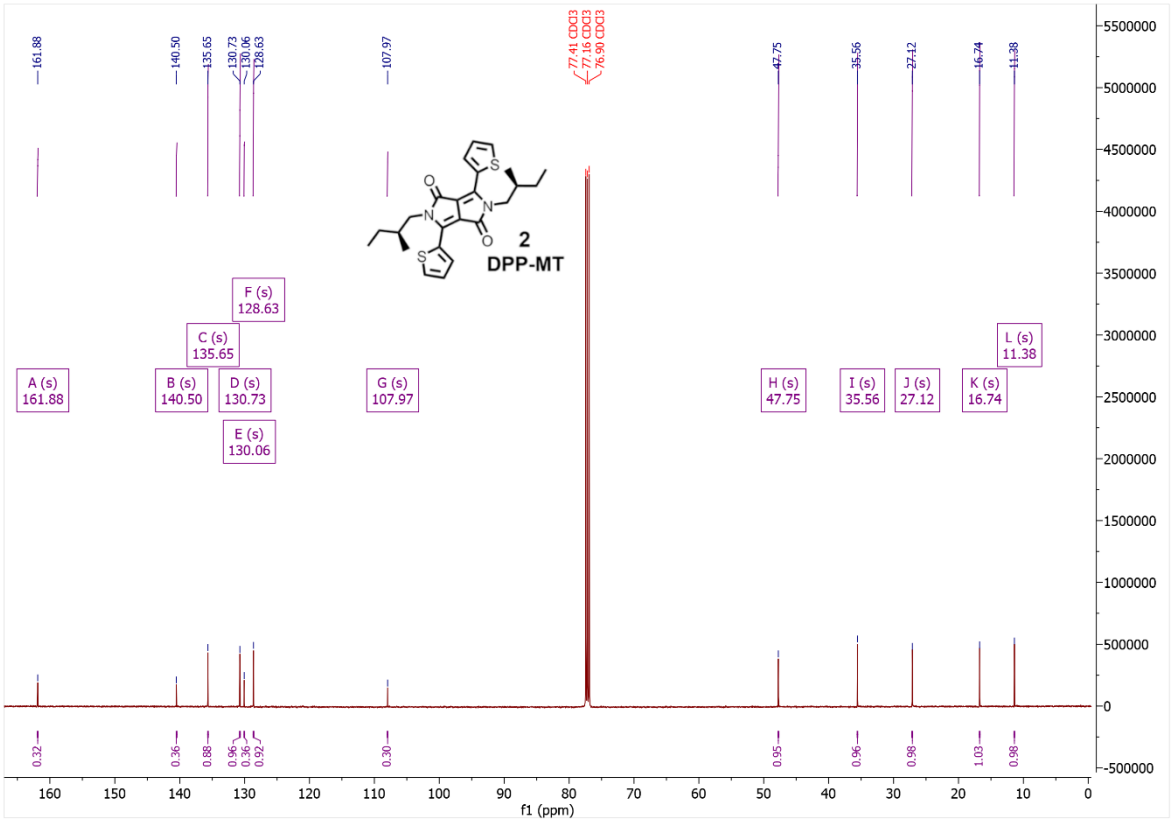

2-((Adamantan-1-yl)methyl)-5-((*S*)-3,7-dimethyloct-6-en-1-yl)-3,6-di(thio-phen-2-yl)-2,5-dihydro-pyrrolo[3,4-*c*]pyrrole-1,4-dione (DPP-ACT, 3):

^{1}H-NMR (500 MHz, $CDCl_3$)

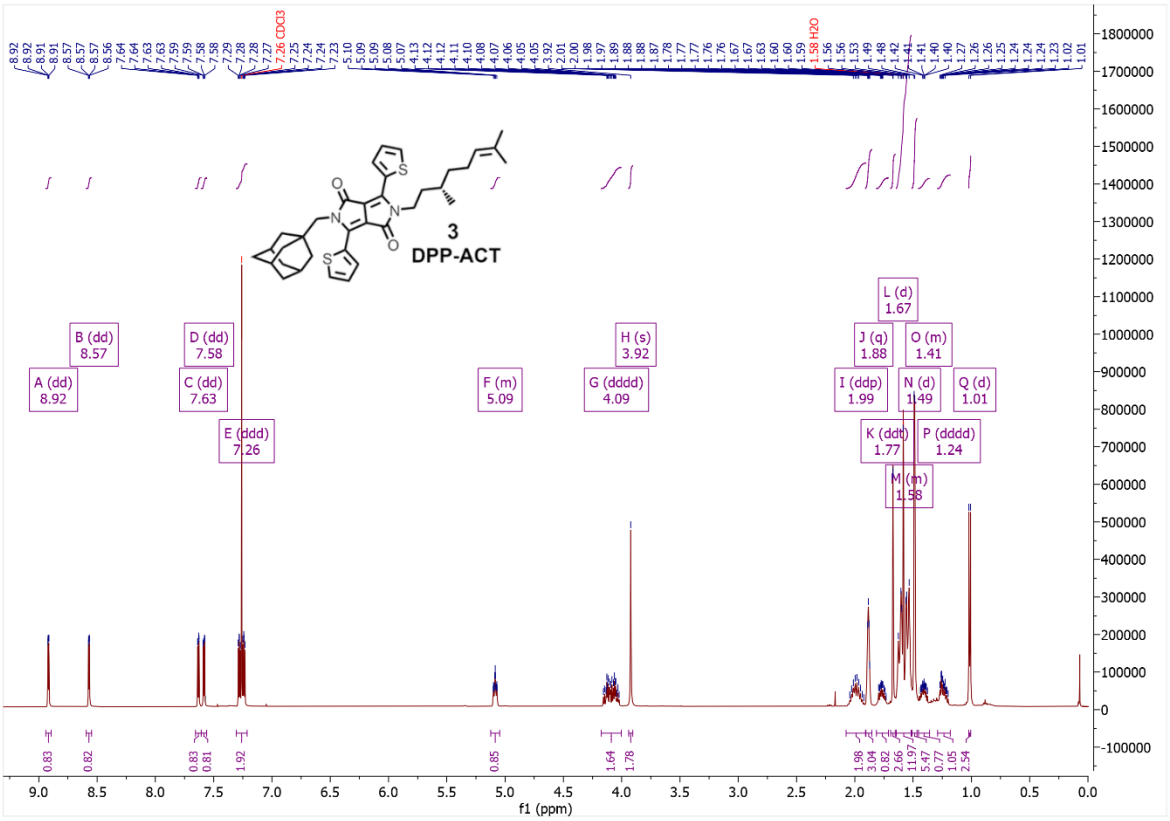

^{13}C-NMR (126 MHz, $CDCl_3$)

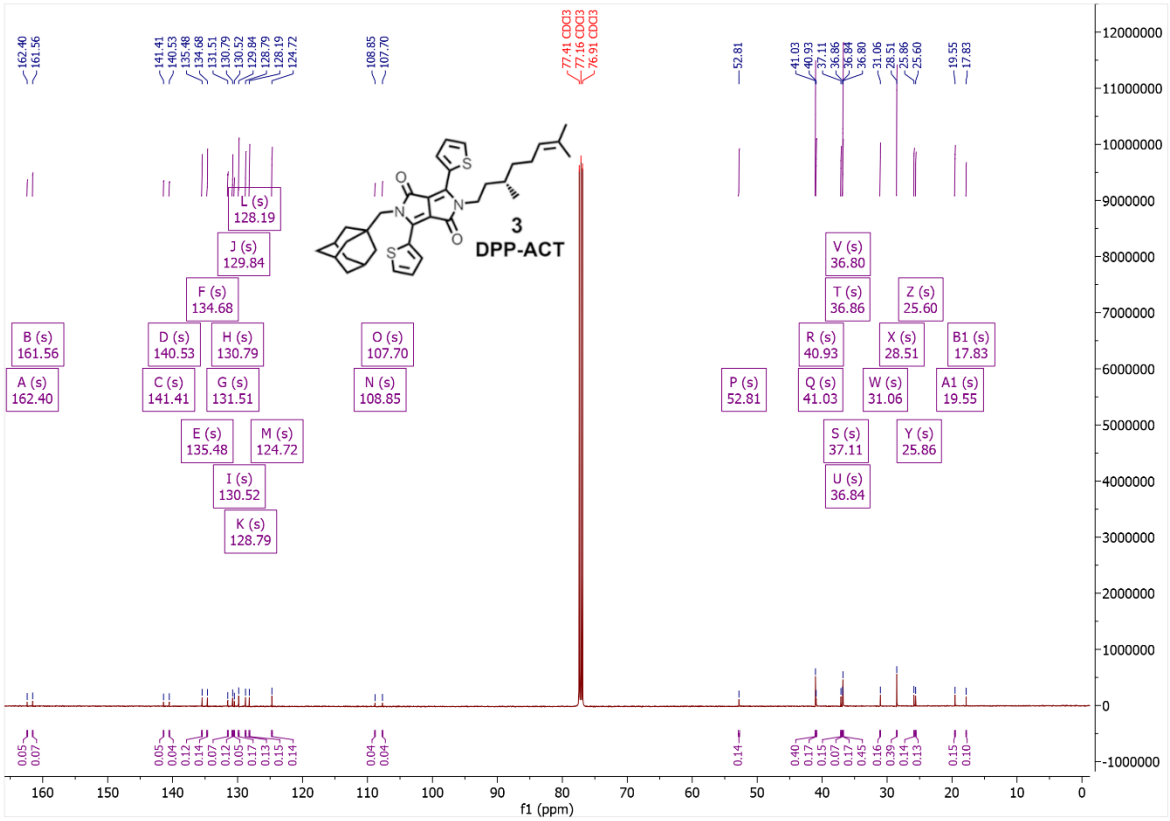

2-((Adamantan-1-yl)methyl)-5-((*S*)-2-methylbutyl)-3,6-di(thiophen-2-yl)-2,5-dihydropyrrolo[3,4-*c*]pyrrole-1,4-dione (DPP-AMT, 4):

^{1}H-NMR (500 MHz, $CDCl_3$)

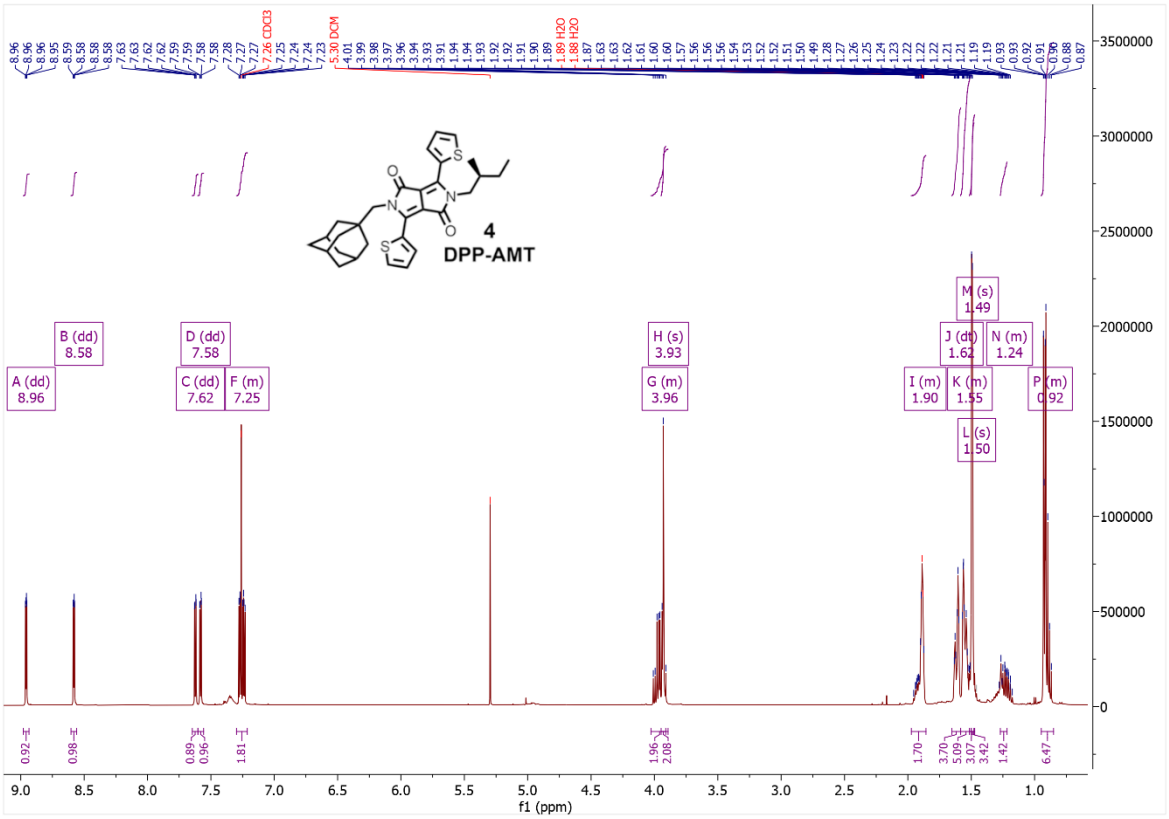

^{13}C-NMR (126 MHz, $CDCl_3$)

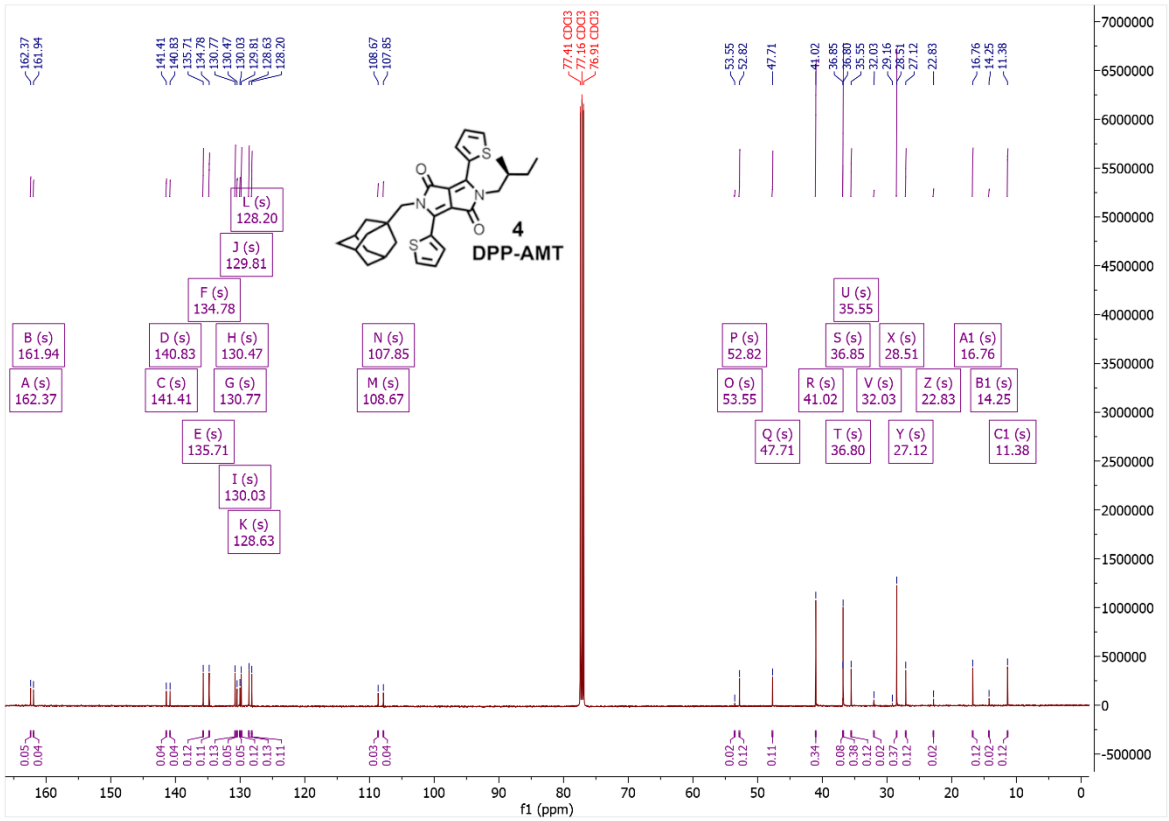

Atomic Coordinates of Optimized Geometries

Model compound **DPP-Me**, *trans* isomer

Single point energy -1673.617897 Hartree, no imaginary frequencies

Symbol	X	Y	Z
N	1.6680950	1.3340960	0.0000000
C	0.3344250	1.7284880	0.0000000
C	-0.4321160	0.5658370	0.0000000
C	0.4321160	-0.5658370	0.0000000
C	1.7965320	-0.0975710	0.0000000
C	-0.3344250	-1.7284880	0.0000000
N	-1.6680950	-1.3340960	0.0000000
C	-1.7965320	0.0975710	0.0000000
C	-0.1478840	3.0811420	0.0000000
C	-1.4866270	3.4416760	0.0000000
C	-1.6900320	4.8405930	0.0000000
C	-0.5193580	5.5517730	0.0000000
S	0.8645360	4.5222360	0.0000000
H	-2.2784230	2.7030180	0.0000000
H	-2.6665660	5.3048950	0.0000000
H	-0.3838250	6.6223790	0.0000000
C	0.1478840	-3.0811420	0.0000000
C	1.4866270	-3.4416760	0.0000000
C	1.6900320	-4.8405930	0.0000000
C	0.5193580	-5.5517730	0.0000000
S	-0.8645360	-4.5222360	0.0000000
H	2.2784230	-2.7030180	0.0000000
H	2.6665660	-5.3048950	0.0000000
H	0.3838250	-6.6223790	0.0000000
O	2.8816690	-0.6618630	0.0000000
O	-2.8816690	0.6618630	0.0000000
C	2.8576460	2.1648980	0.0000000
H	3.7070630	1.4830930	0.0000000
H	2.9049260	2.7924120	0.8924070
H	2.9049260	2.7924120	-0.8924070
C	-2.8576460	-2.1648980	0.0000000
H	-3.7070630	-1.4830930	0.0000000
H	-2.9049260	-2.7924120	-0.8924070
H	-2.9049260	-2.7924120	0.8924070

Model compound **DPP-Me**, *cis* isomer

Single point energy -1673.610738 Hartree, no imaginary frequencies

Symbol	X	Y	Z
N	1.8194160	1.1183880	0.0213060
C	0.5383490	1.6709950	0.0027550
C	-0.3591800	0.6155700	-0.0716020
C	0.3591800	-0.6155700	-0.0716020
C	1.7744460	-0.3175070	-0.0315530
C	-0.5383490	-1.6709950	0.0027550
N	-1.8194160	-1.1183880	0.0213060
C	-1.7744460	0.3175070	-0.0315530
C	0.2718620	3.0818030	0.0782260
C	1.0998420	4.1203950	0.4758460
C	0.4734820	5.3870730	0.4327150
C	-0.8246700	5.3156820	-0.0022630
S	-1.3173110	3.7024970	-0.3459060
H	2.1133950	3.9792710	0.8137370
H	0.9604840	6.3101370	0.7156430
H	-1.5280470	6.1244980	-0.1292590
C	-0.2718620	-3.0818030	0.0782260
C	-1.0998420	-4.1203950	0.4758460
C	-0.4734820	-5.3870730	0.4327150
C	0.8246700	-5.3156820	-0.0022630
S	1.3173110	-3.7024970	-0.3459060
H	-2.1133950	-3.9792710	0.8137370
H	-0.9604840	-6.3101370	0.7156430
H	1.5280470	-6.1244980	-0.1292590
O	2.7763060	-1.0116310	-0.0626660
O	-2.7763060	1.0116310	-0.0626660
C	3.0962400	1.7995130	-0.0811860
H	3.8305620	1.0447130	-0.3599520
H	3.4003240	2.2362640	0.8736100
H	3.0592470	2.5775450	-0.8447310
C	-3.0962400	-1.7995130	-0.0811860
H	-3.8305620	-1.0447130	-0.3599520
H	-3.0592470	-2.5775450	-0.8447310
H	-3.4003240	-2.2362640	0.8736100